New 2-Arylpyrazolo[3,4-*c*]quinoline Derivatives as Potent and Selective Human A_3 Adenosine Receptor Antagonists. Synthesis, Pharmacological Evaluation, and Ligand−Receptor Modeling Studies

Vittoria Colotta,*[,†] Daniela Catarzi,[†] Flavia Varano,[†] Francesca Capelli,[†] Ombretta Lenzi,[†] Guido Filacchioni,[†] Claudia Martini,[‡] Letizia Trincavelli,[‡] Osele Ciampi,[‡] Anna Maria Pugliese,[§] Felicita Pedata,[§] Andrea Schiesaro,[||] Erika Morizzo,[||] and Stefano Moro[||]

Dipartimento di Scienze Farmaceutiche, Laboratorio di Progettazione, Sintesi e Studio di Eterocicli Biologicamente Attivi, Università di Firenze, Polo Scientifico, Via Ugo Schiff, 6, 50019 Sesto Fiorentino, Italy, Dipartimento di Psichiatria, Neurobiologia, Farmacologia e Biotecnologie, Università di Pisa, Via Bonanno, 6, 56126 Pisa, Italy, Dipartimento di Farmacologia Preclinica e Clinica, Università di Firenze, Viale Pieraccini 6, 50139 Firenze, and Molecular Modeling Section, Dipartimento di Scienze Farmaceutiche, Università di Padova, Via Marzolo 5, 35131 Padova, Italy

Received January 31, 2007

This paper reports the study of some 2-arylpyrazolo[3,4-*c*]quinolin-4-ones, 4-amines, and 4-amino-substituted derivatives designed as human A_3 adenosine receptor (AR) antagonists. Most of the herein reported compounds showed a nanomolar affinity toward the hA_3 receptor subtype and different degrees of selectivity that resulted to be strictly dependent on the presence and nature of the substituent on the 4-amino group. Bulky and lipophilic acyl groups, as well as the benzylcarbamoyl residue, afforded highly potent and selective hA_3 receptor antagonists. The selected 4-diphenylacetylamino-2-phenylpyrazoloquinoline (**25**) and 4-dibenzoylamino-2-(4-methoxyphenyl)pyrazoloquinoline (**36**), tested in an in vitro rat model of cerebral ischemia, prevented the irreversible failure of synaptic activity induced by oxygen and glucose deprivation in the hippocampus. The observed structure−affinity relationships of this class of antagonists were also exhaustively rationalized using the recently published ligand-based homology modeling (LBHM) approach.

Introduction

The purine nucleoside adenosine modulates a wide variety of physiological processes, both in the central nervous system and in the periphery, through activation of cell surface receptors belonging to the superfamily of G protein-coupled receptors (GPCRs[a]). Up to now, four subtypes of adenosine receptors (ARs), referred to as A_1, A_{2A}, A_{2B} and A_3, have been identified and cloned.[1,2] Activation of ARs causes adenylyl cyclase inhibition (A_1 and A_3) or stimulation (A_{2A} and A_{2B}),[1] although it is now apparent that other intracellular signaling pathways can be induced. Indeed, the A_1 AR can activate different types of K^+ channels and inhibit Q-, P-, and N-type Ca^{2+} channels,[1] and the A_3 AR subtype is positively coupled to phospholiphase C[3] and D,[4] K_{ATP} channels,[5] and calcium mobilization.[5,6] Greater understanding of the physiological roles of the various AR subtypes provides increasing evidence that these receptors could be challenging druggable targets in a host of pathological conditions.[7,8] Indeed, selective AR antagonists are demonstrating to be potentially useful as therapeutic agents in a wide variety of diseases. In particular, A_1 AR antagonists are effective as diuretic agents[9,10] and also show neuroprotective activity in animal models of in vivo ischemia.[11] Recently, significant anxiolitic and cognitive-enhancing activities were exhibited by the pyrazolopyridine FR194921, a potent, selective, centrally active A_1 AR antagonist.[12] A_3 AR antagonists are being investigated as potential agents against renal injury[13] and also as neuroprotective agents.[14,15] However, it has to be noted that involvement of the A_3 AR in regulation of the cell cycle may afford both cell protection and cell death, being highly dependent on the cell- or tissue-specific context associated with the pathophysiological condition and/or the degree of receptor activation.[11,14,16] Recent studies indicated that A_3 AR antagonists could have a potential therapeutic role in the treatment of glioblastoma multiforme.[17]

Over the past decade, part of our research has been aimed at finding new AR antagonists and, toward this purpose, we have investigated different classes of closely correlated tricyclic compounds.[18−25] One of these classes is represented by the 2-arylpyrazolo[3,4-*c*]quinolin-4-ones and the corresponding 2-arylpyrazolo[3,4-*c*]quinolin-4-amines (Chart 1).[18] In both the 4-oxo and 4-amino series, small substituents at the R position on the 2-phenyl ring (R = 4-Me, 3-Me, 4-OMe) ameliorated the hA_3 AR binding affinity. Moreover, a significant difference was observed between the two series: most of the 4-one derivatives demonstrated a human (h) A_3 AR affinity in the low nanomolar range (K_i = 3−30 nM), while the corresponding 4-amino compounds were about 20−60 fold less active. Interestingly, the hA_3 receptor affinity of the 2-phenylpyrazolo[3,4-*c*]quinolin-4-amine (K_i = 550 nM) was enhanced to the low nanomolar range when acyl residues or the benzylcarbamoyl moiety were appended on the 4-amino group.

Together, these results showed that the 2-phenylpyrazolo[3,4-*c*]quinoline scaffold possesses good electronic and steric

* Corresponding author. Tel: +39 55 4573731. Fax: +39 55 4573780. E-mail: vittoria.colotta@unifi.it.

[†] Dipartimento di Scienze Farmaceutiche, Università di Firenze.

[‡] Università di Pisa.

[§] Dipartimento di Farmacologia Preclinica e Clinica, Università di Firenze.

[||] Università di Padova.

[a] Abbreviations: GPCRs, G protein-coupled receptors; AR, adenosine receptor; h, human; r, rat; I-AB-MECA, N^6-(4-amino-3-iodobenzyl)-5′-(*N*-methylcarbamoyl)adenosine; NECA, 5′-(*N*-ethylcarboxamido)adenosine; DPCPX, 8-cyclopentyl-1,3-dipropylxanthine; CGS 21680, 2-[4-(2-carboxyethyl)phenethyl]amino-5′-(*N*-ethylcarbamoyl)adenosine; R-PIA, (*R*)-N^6-(2-phenylisopropyl)adenosine; OGD, oxygen and glucose deprivation; AD, anoxic depolarization; fepsp, field excitatory post sinaptic potential; dc, direct current; aCSF, artificial cerebral spinal fluid; TM, transmembrane; EL2, second extracellular loop; RBHM, rhodopsin-based homology modeling; LBHM, ligand-based homology modeling; MOE, molecular operating environment.

10.1021/jm070123v CCC: $37.00
Published on Web 08/01/2007

Chart 1. Previously Reported Pyrazolo[3,4-*c*]quinolin-4-ones and 4-Amines

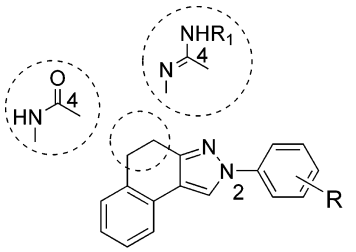

properties for anchoring to the hA_3 receptor recognition site. On this basis, we decided to continue the study of this class of compounds in order to further investigate the structure−activity relationships (SAR) and gain more insight about the pattern of substitution that may afford high hA_3 affinity and selectivity. Thus, we report some 4-oxo-, 4-amino-, 4-amido-, and 4-benzylureido-pyrazoloquinoline derivatives (**1**−**36**, Chart 2) that were tested to evaluate their affinities at hA_1, hA_{2A}, and hA_3 ARs. Two selected derivatives, 4-diphenylacetylamino-2-phenylpyrazoloquinoline (**25**) and 4-dibenzoylamino-2-(4-methoxyphenyl)pyrazoloquinoline (**36**), were also tested in an in vitro rat model of cerebral ischemia to assess their efficacy in preventing the irreversible failure of synaptic activity induced by oxygen and glucose deprivation.

Molecular modeling studies were carried out on this class of pyrazolo[3,4-*c*]quinolines in order to rationalize their hA_3 AR affinity data and depict their putative binding mode. Thus, the herein reported derivatives were docked to our improved model of the hA_3 AR recognition site.[22−30]

Chemistry

Synthesis of the pyrazolo[3,4-*c*]quinolin-4-ones **1**−**4** and **7** has already been reported.[31] In the present work these compounds were resynthesized following the previously reported pathway (Scheme 1) but employing microwave irradiation rather than conventional heating. Briefly, a mixture of 3-ethoxalylindole[32] with the suitable hydrazine hydrochloride in absolute ethanol and a few drops of glacial acetic acid was microwave irradiated at 140 °C for 3 min to afford the desired pyrazolo[3,4-*c*]quinolin-4-ones **1**−**4** and **7**. Compared to the conventional method, the microwave-assisted procedure afforded the desired

Scheme 1[a]

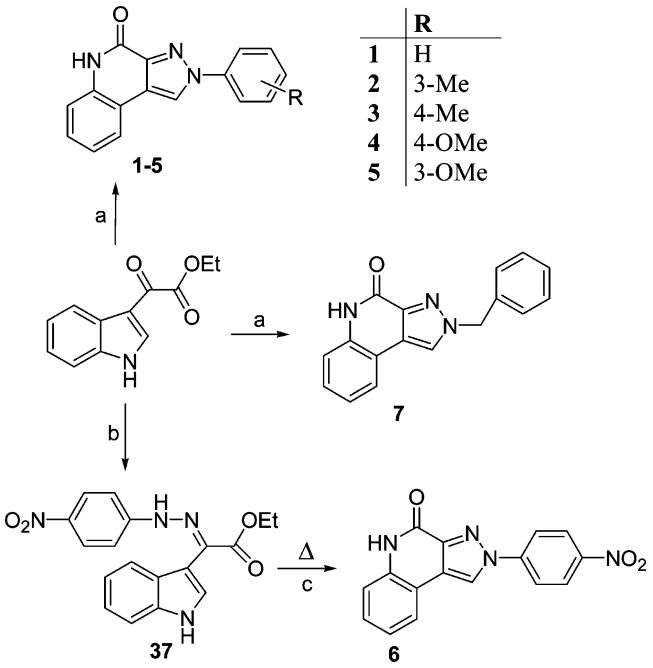

	R
1	H
2	3-Me
3	4-Me
4	4-OMe
5	3-OMe

[a] (a) Arylhydrazine hydrochloride or benzylhydrazine dihydrochloride, absolute EtOH, AcOH, microwave irradiation; (b) 4-nitrophenylhydrazine, EtOH, AcOH, conc HCl, reflux; (c) neat, $T = 230$ °C.

compounds in a shorter time with improved yields. Thus, the microwave procedure was employed to prepare the new 2-(3-methoxyphenyl)pyrazolo[3,4-*c*]quinolin-4-one **5**. When 3-ethoxalylindole[32] was reacted with 4-nitrophenylhydrazine hydrochloride, under irradiation at 150 °C for 15 min, a mixture of compound **6** and its hydrazone precursor **37** (ratio 2:1, ^{1}H NMR spectrum) was obtained. Thus, we prepared **6** following the conventional method. Reaction of 3-ethoxalylindole[32] with 4-nitrophenylhydrazine in refluxing absolute ethanol, glacial acetic acid, and hydrochloric acid gave the hydrazone **37** that was cyclized by heating at 230 °C.

Synthesis of the 2-arylpyrazolo[3,4-*c*]quinolin-4-amines **8**−**11** is reported in ref 18, and following the same method we prepared the new 2-(3-methoxyphenyl)pyrazolo[3,4-*c*]quinolin-4-amine (**12**) (Scheme 2). Briefly, the 4-oxo derivative **5** was reacted with a mixture of phosphorus pentachloride/phosphorus oxychloride to give the corresponding 4-chloro derivative **38**,

Chart 2. Herein Reported 2-Arylpyrazolo[3,4-*c*]quinolines

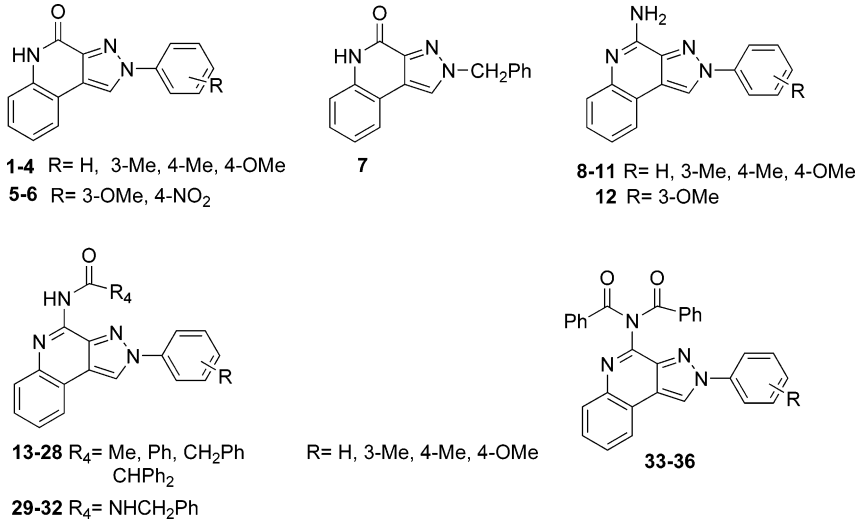

Scheme 2[a]

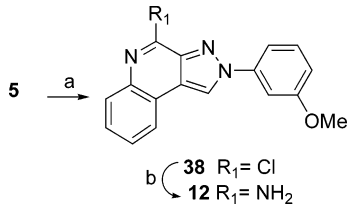

[a] (a) $PCl_5/POCl_3$; (b) NH_3(g), absolute EtOH.

which was transformed into the desired 4-amino derivative **12** with ammonia. The synthesis of the 2-phenylpyrazolo[3,4-*c*]-quinoline derivatives (R = H) bearing the 4-acetylamino (**13**), 4-benzoylamino (**17**), 4-phenylacetylamino (**21**), and 4-benzylureido (**29**) substituents was previously described.[18] The new 2-arylpyrazolo[3,4-*c*]quinolin-4-acylamines **14**−**16**, **18**−**20**, **22**−**24**, **25**−**28** (Scheme 3) were prepared by reacting the corresponding 2-arylpyrazolo[3,4-*c*]quinolin-4-amines **8**−**11** and the suitable carboxylic acids in dimethylformamide and in the presence of 1-hydroxybenzotriazole, trietylamine, and 4-(dimethylamino)pyridine. The 2-arylpyrazolo[3,4-*c*]quinolin-4-benzylureides **30**−**32** (Scheme 3) were obtained by refluxing derivatives **9**−**11** and benzyl isocyanate in anhydrous tetrahydrofuran. The 2-arylpyrazolo[3,4-*c*]quinolin-4-dibenzoylamines **33**−**36** (Scheme 3) were synthesized by treatment of the 4-amino derivatives **8**−**11** with an excess of benzoyl chloride in anhydrous methylene chloride and pyridine.

Pharmacology

Derivatives **5**−**7**, **12**, **14**−**16**, **18**−**20**, **22**−**28**, and **30**−**36** were tested for their ability to displace [^{125}I]AB-MECA from cloned hA_3 AR. These derivatives, and the previously reported hA_3 AR antagonists **1**−**4**, **8**−**11**, **17**, and **29**, were tested for their ability to displace [^{3}H]DPCPX and [^{3}H]NECA, respectively, from cloned hA_1 and hA_{2A} ARs stably expressed in CHO cells. The binding results of **1**−**36**, together with those of theophylline and DPCPX included as reference antagonists, are reported in Table 1. To evaluate their hA_3 AR antagonistic effect, the two selected compounds **25** and **36** were tested for their ability to counteract the NECA-mediated inhibition of cAMP accumulation in CHO cells stably expressing hA_3 AR (Figure 1). Derivatives **25** and **36** were also tested to evaluate their affinities at rat (r) A_1, A_{2A}, and A_3 ARs. The rA_1 and rA_{2A} AR affinities were evaluated using [^{3}H]DPCPX (rat cortex) and [^{3}H]CGS 21680 (rat striatum), respectively. The rA_3 receptor binding affinity was determined by competition experiments using [^{3}H](R)-PIA in rat testis membranes, in the presence of DPCPX to block A_1 binding sites.

Compounds **25** and **36** were tested to evaluate their effects in an in vitro rat model of cerebral ischemia obtained by oxygen and glucose deprivation (OGD). The results of these studies are reported in Figure 2.

Results and Discussion

(A) Structure−**Affinity Relationship Studies.** First of all, it has to be pointed out that the hA_3 AR affinities of the 4-oxo (**1**−**4**), 4-amino (**8**−**11**), 4-acylamino (**13**, **17**, **21**), and 4-benzylcarbamoylamino (**29**) derivatives were reported in a previous paper.[18] In the present work, these derivatives were assayed at human A_1 and A_{2A} ARs in order to establish their hA_3 receptor selectivities. In addition, hA_1 and hA_{2A} receptor affinities of the previously reported compounds were necessary to better

Scheme 3[a]

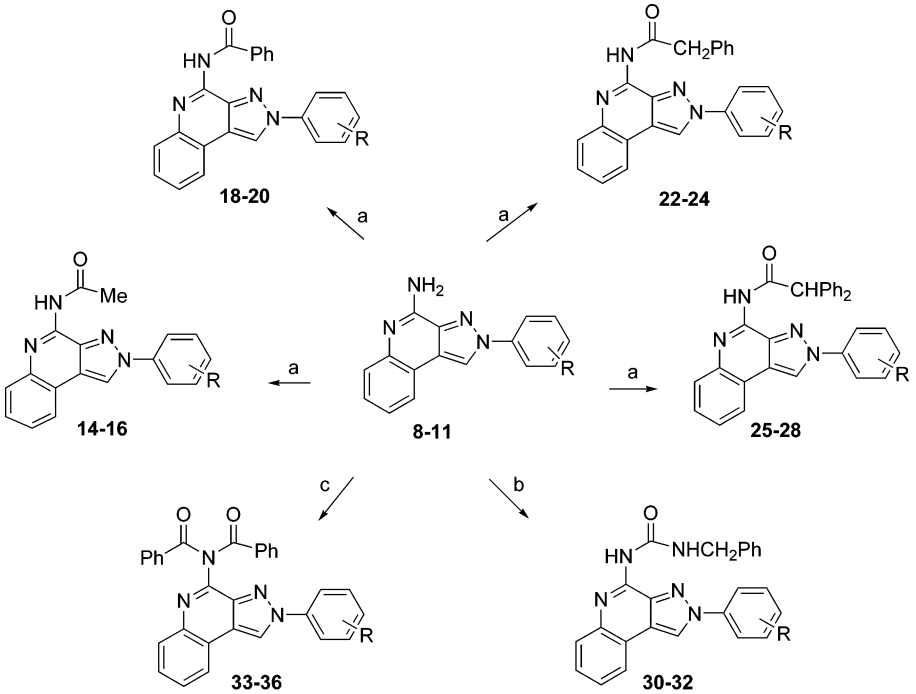

	R
8, 25, 33	H
9, 14, 18, 22, 26, 30, 34	3-Me
10, 15, 19, 23, 27, 31, 35	4-Me
11, 16, 20, 24, 28, 32, 36	4-OMe

[a] (a) Suitable carboxylic acid, 1-hydroxybenzotriazole, NEt_3, 4-(dimethylamino)pyridine, 1-(3-(dimethylamino)propyl)-3-ethylcarbodiimide hydrochloride, DMF; (b) benzyl isocyanate, THF; (c) PhCOCl, anhydrous pyridine, methylene chloride.

Table 1. Binding Activity at Human A_1, A_{2A}, and A_3 Adenosine Receptors

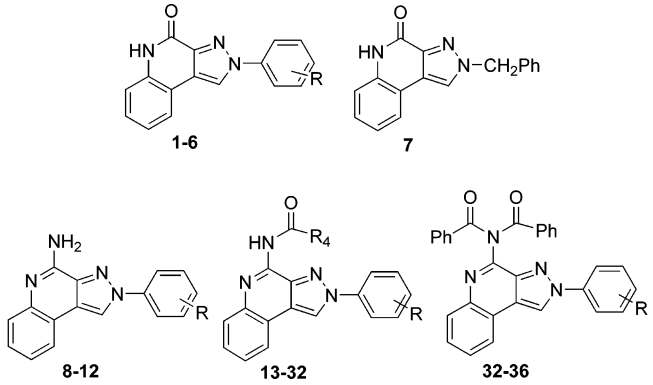

			K_i[a] (nM) or *I*%		
	R	R4	hA_3[b]	hA_1[c]	hA_{2A}[c]
1[d]	H		30.8 ± 2.6	203 ± 12	43%
2[d]	3-Me		5.0 ± 0.4	12 ± 1	46%
3[d]	4-Me		3.2 ± 0.2	29 ± 0.5	44%
4[d]	4-OMe		3.2 ± 0.2	176.4 ± 8.8	25%
5	3-OMe		7.3 ± 0.1	14 ± 0.4	52%
6	4-NO_2		85.5 ± 4	357 ± 35	0%
7			74.5 ± 5.3	8%	32%
8[d]	H		551 ± 34	659 ± 43	91 ± 7.3
9[d]	3-Me		99.3 ± 7.8	21 ± 1.6	228 ± 12.3
10[d]	4-Me		188 ± 15	45 ± 3.4	329 ± 22
11[d]	4-OMe		90.2 ± 7.3	40 ± 3.1	1060 ± 96
12	3-OMe		228.5 ± 19	32 ± 3.0	486 ± 34
13[d]	H	Me	48.2 ± 3.5	0%	3%
14	3-Me	Me	31 ± 2.4	203 ± 15	10%
15	4-Me	Me	123 ± 10	455 ± 41	1500 ± 130
16	4-OMe	Me	101.5 ± 7.4	2875 ± 110	0%
17[d]	H	Ph	2.1 ± 0.1	0%	9%
18	3-Me	Ph	4.3 ± 0.5	57 ± 4.2	2860 ± 224
19	4-Me	Ph	4.4 ± 0.2	629 ± 51	26%
20	4-OMe	Ph	3.4 ± 0.2	250 ± 13	39%
21[d]	H	CH_2Ph	9.9 ± 0.8	5%	15%
22	3-Me	CH_2Ph	3.9 ± 0.3	60 ± 4.5	24%
23	4-Me	CH_2Ph	5.6 ± 0.4	55%	21%
24	4-OMe	CH_2Ph	4.5 ± 0.6	201 ± 12	51%
25	H	$CHPh_2$	8.9 ± 0.6	0%	21%
26	3-Me	$CHPh_2$	14 ± 1.5	559 ± 42	4%
27	4-Me	$CHPh_2$	11.5 ± 1.3	32%	3%
28	4-OMe	$CHPh_2$	9 ± 0.5	47%	0%
29[d]	H	$NHCH_2Ph$	8.3 ± 0.7	0%	3%
30	3-Me	$NHCH_2Ph$	3.35 ± 0.2	6800 ± 510	20%
31	4-Me	$NHCH_2Ph$	257 ± 21	5%	39%
32	4-OMe	$NHCH_2Ph$	40%	43%	0%
33	H		6.1 ± 0.5	0%	0%
34	3-Me		23.25 ± 2.1	42%	20%
35	4-Me		30 ± 2.3	32%	0%
36	4-OMe		17.2 ± 1.4	25%	7%
theophylline			86000 ± 7800	6200 ± 530	7900 ± 630
DPCPX			1300 ± 125	3.2 ± 0.2	260 ± 18

[a] The K_i values are means ± SEM of four separate assays, each performed in triplicate. [b] Displacement of specific [^{125}I]AB-MECA binding at human A_3 receptors expressed in CHO cells or percentage of inhibition (*I*%) of specific binding at 1 μM concentration. [c] Displacement of specific [^{3}H]DPCPX and [^{3}H]NECA binding at, respectively, hA_1 and hA_{2A} receptors expressed in CHO cells or percentage of inhibition (*I*%) of specific binding at 10 μM concentration. [d] The hA_3 AR binding affinity was reported in ref 18.

outline the structure−selectivity relationships of the newly synthesized pyrazoloquinolines.

The 4-oxo derivatives **1**−**7** do not bind to the hA_{2A} receptor while all the 4-amino derivatives **8**−**12**, and in particular the 2-phenyl substituted compound **8**, possess good hA_{2A} AR affinities. The previously reported 4-one derivatives **1**−**4**, which turned out to be highly potent at the hA_3 receptor,[18] show quite good affinities at the hA_1 AR and, indeed, scarce hA_3 vs hA_1 selectivity. Among the previously investigated R substituents (compounds **1**−**4**), the *p*-methoxy group was the most profitable for both the hA_3 affinity and hA_3 vs hA_1 selectivity. Thus, we decided to move it from the para to the meta position (compound **5**) in order to evaluate whether this shift could optimize anchoring to the hA_3 receptor site (the ortho position was not investigated since our previous results indicated that it was an unfavorable position).[18] This modification left the hA_3 AR affinity almost unchanged but significantly increased that at the hA_1 AR, thus annulling the hA_3 vs hA_1 receptor selectivity. In contrast, compound **5** was inactive at the hA_{2A} AR.

The new 2-(4-nitrophenyl)pyrazolo[3,4-*c*]quinolin-4-one (**6**) was synthesized since the presence of the *p*-nitro group on the 2-phenyl moiety of our 1,2,4-triazolo[4,3-*a*]quinoxalin-1,4-dione

series[22] afforded subnanomolar hA_3 receptor affinity and high selectivity. Instead, this substituent did not exert the same profitable effects in the pyrazoloquinoline series, since compound **6** shows the lowest affinity (K_i = 85 nM), among the 4-oxo derivatives, and also low hA_3 vs hA_1 selectivity. These results discouraged us from performing the same modification on the 4-amino series.

Movement of the lipophilic 2-phenyl moiety away from the pyrazoloquinoline nucleus gave rise to 1-benzylpyrazolo[3,4-*c*]quinolin-4-one (**7**), which still maintains a nanomolar hA_3 AR affinity, although 10-fold lower than that of the 2-phenyl derivative **1**. This result indicates that the receptor pocket, where the 2-appended moiety of these derivatives is accommodated, is roomy enough to hold the rather bulky benzyl group. In contrast, the hA_1 receptor pocket seems to have a lower bulk tolerance, as compound **7** is totally inactive at this receptor subtype.

The previously reported quinolin-4-amines **8**−**11** showed good hA_3 AR affinities, yet lower (K_i = 90−550 nM) than those of the corresponding 4-oxo substituted compounds **1**−**4** (K_i = 3−30 nM). Differently from the 4-oxo compounds **1**−**4**, the 4-amino derivatives **8**−**11** possess, on the whole, higher affinity at the hA_1 AR than at the hA_3 one. The same applies to the newly synthesized 2-(3-methoxyphenyl)pyrazolo[3,4-*c*]quinolin-4-amine (**12**), which showed a 7-fold higher affinity for the hA_1 receptor (K_i = 32 nM) than for the hA_3 one. Compounds **9**−**12** display some hA_{2A} affinity, although lower than those at the hA_1 and hA_3 ARs. In contrast, the 2-phenylpyrazolo[3,4-*c*]-quinolin-4-amine (**8**) binds the A_{2A} receptor better than the other two subtypes.

Considering the pyrazoloquinoline derivatives **13**−**36**, bearing acyl or carbamoyl moieties on the 4-amino group, we should first point out that we decided to introduce on the 2-phenyl ring the substituents that have led to the best hA_3 AR affinities in the 4-amino derivatives (R = 3-Me, 4-Me, 4-OMe). On the whole, the 4-acylamino compounds **13**−**28**, **33**−**36**, compared to the 4-amino derivatives **8**−**11**, showed a significantly ameliorated hA_3 receptor affinity and a reversed selectivity, possessing generally scarce or null affinities at the hA_1 and hA_{2A} ARs. Only compounds **18** and **22** possess good affinities for the hA_1 receptor. Instead, among the 2-aryl-4-benzylureidopyrazoloquinolines **30**−**32**, only the 2-(3-methylphenyl) derivative **30** binds better at the hA_3 receptor than the corresponding 4-amino parent compound **9**. It has to be noted that the 4-acetylamino derivatives **13**−**16** show lower hA_3 receptor affinities in comparison with all the other 4-acylamino derivatives **17**−**28**, **33**−**36**, which bear more lipophilic and hindering R_4 residues than the acetyl group. These results suggest not only the existence of a roomy receptor pocket, where the R_4 groups are accommodated, but also the importance of hydrophobic interactions between the R_4 substituent and the receptor site.

Analyzing the role of the R substituent on the 2-phenyl ring of the 4-amido derivatives **13**−**28**, **33**−**36**, it can be observed that R maintained but did not ameliorate the high hA_3 affinities of the corresponding 2-phenyl parent derivatives. The effect of R is even disadvantageous on the 4-benzylureido pyrazoloquinolines **29**−**32**. Only the 2-(3-methylphenyl) derivative **30** shows comparable hA_3 affinity to that of the 2-phenyl compound **29**, while the other 2-aryl derivatives are significantly less potent.

As regards the role of the R substituent on the hA_3 versus hA_1 selectivity of the 4-amido/4-ureido-substituted derivatives **13**−**36**, we can observe that R affected the hA_1 affinities differently, depending on the nature of the 4-moiety. In the 2-aryl derivatives **14**−**16** (R_4 = methyl), **18**−**20** (R_4 = phenyl), and **22**−**24** (R_4 = benzyl), the R groups restored some hA_1 receptor affinities with respect to those of the corresponding 2-phenyl derivatives **13**, **17**, and **21**, thus reducing the hA_3 selectivities. In particular, among the probed R substituents, the 3-methyl group turned out to be the worst in terms of hA_3 selectivity, since it afforded the best hA_1 receptor affinities (compounds **14**, **18**, **22**). Instead, in the 4-diphenylacetylamino (**26**−**28**), 4-benzylureido (**30**−**32**), and 4-dibenzoylamino (**34**−**36**) compounds, the R susbstituent, in general, does not affect binding to the hA_1 receptor, all these 2-aryl derivatives being as inactive as the corresponding 2-phenyl derivatives **25** and **29**.

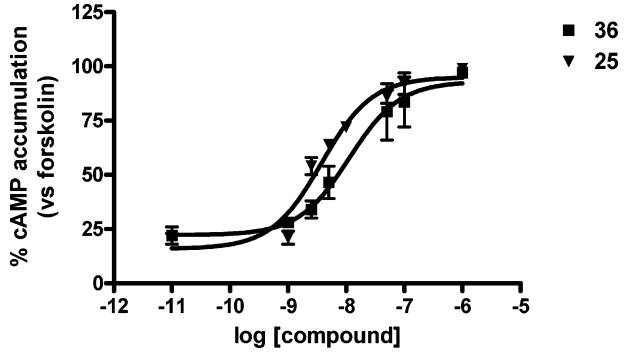

Figure 1. Effect of compounds **25** and **36** on NECA-mediated cAMP accumulation (vs forskolin, set to 100%) in CHO cells stably expressing hA_3 AR. Data represents the mean ± SEM from three separate experiments. The EC_{50} values for **36** and **25** were 11.2 ± 1.2 and 3.8 ± 0.41 nM, respectively.

The two selected compounds **25** and **36**, which showed high hA_3 AR affinities and selectivities, were tested to evaluate their inhibitory effects on NECA-modulated cAMP accumulation in CHO cells expressing the hA_3 receptor (Figure 1). The antagonistic potencies of compounds **25** (EC_{50} = 3.8 nM) and **36** (EC_{50} = 11.2 nM) are in accordance with their hA_3 AR affinity values.

As expected, receptor affinities of compounds **25** and **36** were lower at the rA_3 AR than at the hA_3 AR. In fact, displacement of the radioligand binding at the rA_3 receptor by compounds **25** and **36**, at 1 μM concentration, was 30% and 28%, respectively; thus, the rA_3 AR K_i values are expected to fall in the low μM range. Derivatives **25** and **36** showed poor affinities for the rA_{2A} AR since, at 10 μM concentration, they displaced the radioligand by 26% and 2%, respectively. The rA_1 affinity of **36** was also very low (I = 11% at 10 μM), while that of compound **25** was moderate (K_i = 1491 ± 147 nM).

(B) Electrophysiological Studies. Compounds **25** and **36** were pharmacologically evaluated in an in vitro rat model of cerebral ischemia, obtained by OGD. This experimental condition is aimed at reproducing in vitro the consequences of interruption of blood flow following cardiac arrest or occlusion of intracranial vessels. The affinity value of adenosine to the rat A_3 receptors in binding experiments is 6.5 μM.[33] Thus, activation of this adenosine receptor subtype requires a higher concentration of adenosine. During hypoxic/ischemic conditions in vivo[34] and in vitro[35] high adenosine extracellular concentrations are reached that are sufficient to activate adenosine A_3 receptors. The harmful role of A_3 receptors during OGD is suggested by the observation that the block of A_3 AR significantly protects against the irreversible disruption of excitatory neurotransmission caused by a severe ischemic episode and consistently abolishes or delays the occurrence of anoxic depolarization (AD).[15] The latter phenomenon is closely cor-

related with the extension of brain damage during ischemia both in vitro and in vivo.[36]

In the present work, we tested compounds **25** and **36** to investigate their effect on synaptic transmission during severe (7-min duration) OGD in the CA1 region of rat hippocampal slices. This brain region is one of the most vulnerable to ischemia, due to pyramidal neuron death.[37]

Figure 2A shows that 7-min OGD is a duration of ischemic insult that induces an irreversible loss of field excitatory postsynaptic potential (fepsp) amplitude (recovery of 5.2 ± 0.3%, $n = 5$). The selective A_3 AR antagonist **36** (100 nM) prevents the deleterious effect of 7-min OGD on neurotransmission, permitting a significant recovery of fepsp amplitude (84 ± 16%, $n = 5$, $P < 0.001$, one-way ANOVA, Newman−Keuls multiple comparison post-hoc test vs control slices). Figure 2B shows that under control conditions 7-min OGD episodes always caused AD, recorded as negative direct current (dc) shifts, with a mean peak latency of 6.2 ± 0.3 min from the beginning of ischemia and a peak amplitude of −8.2 ± 0.5 mV ($n = 5$). In the presence of the A_3 AR antagonist **36** (100 nM, $n = 5$), AD was absent in three out of the five slices recorded. In the remaining two slices, AD was significantly delayed (mean peak latency of 7.6 ± 0.4 min from the beginning of ischemia) with a reduced peak amplitude (−4.7 ± 1.0 mV). Similar results were obtained in the presence of the A_3 AR antagonist **25** (100 nM). In fact, it prevented synaptic impairment and allowed for a significant synaptic recovery within 15 min from OGD interruption (47 ± 24%, $n = 5$, $P < 0.05$, one-way ANOVA, Newman−Keuls multiple comparison post-hoc test, vs control slices) (Figure 2C). The overall effect of compounds **25** and **36** on fepsp recovery after 7-min OGD, compared with that observed in control preparations, is summarized in Figure 2C.

In summary, the application of severe (7-min) OGD elicits a complete and irreversible depression of neurotransmission that persists upon slice reperfusion with oxygenated and glucose-containing artificial cerebral spinal fluid (aCSF) and is accompanied by the appearance of AD, an unequivocal sign of neuronal injury during ischemia.[36] We demonstrated that the newly synthesized compounds **25** and **36**, potent hA_3 receptor antagonists that displayed micromolar affinities for the rA_3 receptor, prevented or delayed the occurrence of AD and significantly protected against irreversible disruption of excitatory neurotransmission caused by severe (7-min) OGD episodes. These results are in agreement with those previously obtained in the same brain region using other potent hA_3 AR antagonists[15] belonging to different chemical classes, such as 3-propyl 6-ethyl-5-[(ethylthio)carbonyl]-2-phenyl-4-propyl-3-pyridinecarboxylate (MRS 1523),[38] *N*-[9-chloro-2-(2-furanyl)-1,2,4-triazolo[1,5-*c*]quinazolin-5-yl]benzeneacetamide (MRS 1220),[39] and 5-[[(4-pyridyl)amino]carbonyl]amino-8-methyl-2-(2-furyl)pyrazolo[4,3-*e*]-1,2,4-triazolo[1,5-*c*]pyrimidine hydrochloride.[40] All these compounds were demonstrated to reduce the OGD deleterious effect at nanomolar concentration although, among them, only the first derivative possessed good affinity for the rA_3 AR ($K_i = 113$ nM),[38] while the other antagonists, as well as the herein reported compounds **25** and **36**, showed lower binding activities at the rA_3 receptor. The apparent discrepancy between the rA_3 binding affinities of compounds **25** and **36** and their protective effect on OGD, observed at 100 nM concentration, might be due to the difference between the binding experiment model and the electrophysiological model. Alternatively, the paucity of A_3 AR in native tissue[41,42] allows one to speculate that occupancy of a substantial fraction of A_3 receptors is required for evoking cell response(s). Thus, the blockage of a relatively small fraction of A_3 receptors may be sufficient to antagonize the effect of endogenous adenosine released during OGD.

(C) Molecular Modeling Studies. Molecular modeling studies were performed on the pyrazoloquinoline derivatives **1**−**36** in order to identify the hypothetical binding motif of this class of 2-arylpyrazolo[3,4-*c*]quinoline derivatives and rationalize the observed SAR. The main issues to be addressed were (i) to clarify the different role of the R substituent on hA_3 affinity and selectivity of the 4-oxo/4-amino compounds **1**−**12** and 4-acylamino/4-benzylureido derivatives **13**−**36** and (ii) to interpret the advantageous effect of the 4-acylamino moieties both for hA_3 affinity and selectivity.

Following our previously reported modeling studies,[22−25] we have constructed a refined model of the hA_3 receptor by using a rhodopsin-based homology modeling (RBHM) approach.[26−29] Moreover, our recently described ligand-based homology mod-

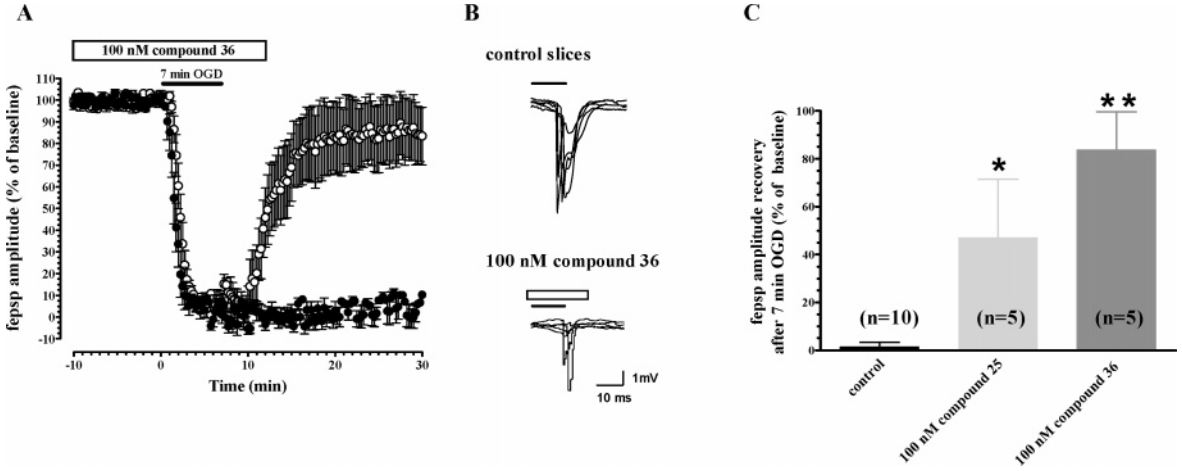

Figure 2. The A_3 adenosine receptor antagonist **36** protects CA1 hippocampus from irreversible fepsp depression induced by 7-min OGD. (A) The time-course of 7-min OGD effect on fepsp amplitude, expressed as percent of baseline, in control aCSF (filled circles; mean ± SEM, $n = 5$) and in the presence of 100 nM **36** (open bar, unfilled circles, mean ± SEM, $n = 5$). (B) AD recorded as the negative dc shift in response to 7-min OGD (solid bars) under control conditions ($n = 5$) and in the presence of compound **36** (100 nM, open bar, $n = 5$). Note that compound **36** blocked AD appearance in three out of five slices and delayed the latency in the other two slices. (C) Column bars indicate the average recovery (mean ± SEM) of fepsps after 7-min OGD, recorded at 15 min reperfusion in aCSF, under control conditions or in the presence of compounds **25** and **36**. $*P < 0.05$, $**P < 0.001$, one-way ANOVA, Newman−Keuls multiple comparison post-hoc test, vs control group.

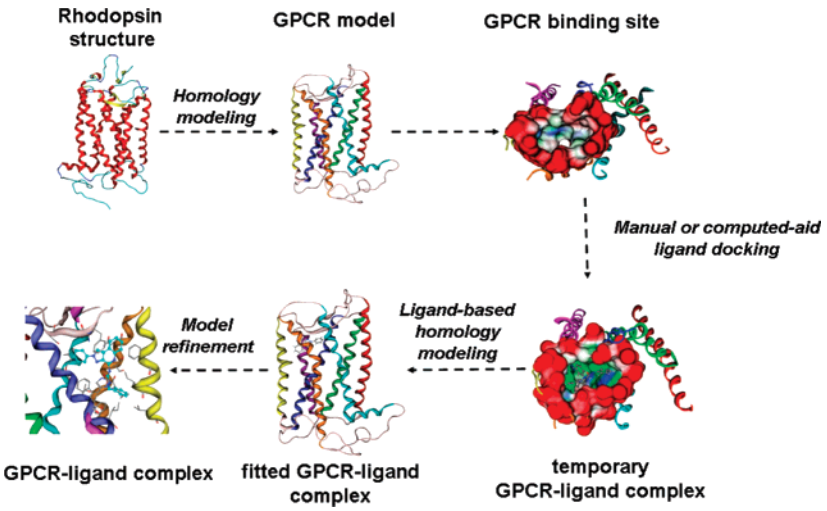

Figure 3. Flow chart of the ligand-based homology modeling technique considering an evolution of a conventional homology modeling algorithm.

eling (LBHM) approach has been used to simulate the conformational changes induced by ligand binding, and a schematic representation of the ligand-based homology protocol is in Figure 3 (methodological details are summarized in the Experimental Section).[30] As reported in Figure 4, depending on the topological properties of the different ligands, we found four different conformational models of the human A_3 receptor reverse agonist-like state in which both shape and chemical complementarities have been specifically optimized around each ligand. In this specific case, with the varying of ligand structure, the molecular volume of the transmembrane (TM) binding cavity changes from the 660 Å^3 of the standard RBHM-driven model to the 1120 Å^3 of the largest LBHM-driven model, without altering the conventional rhodopsin-like receptor topology. The modifications of both shape and volume of the human A_3 TM binding cavity are the most important receptor modeling perturbations obtained by the application of the LBHM technique. The binding cavity reorganization induced by ligand binding is due to the conformational change in several amino acid side chains, such as Leu90 (3.32), Leu91 (3.33), Thr94 (3.36), His95 (3.37), Ile98 (3.40), Gln167 (EL2), Phe168 (EL2), Phe182 (5.43), Ile186 (5.47), Leu190 (5.51), Phe239 (6.44),

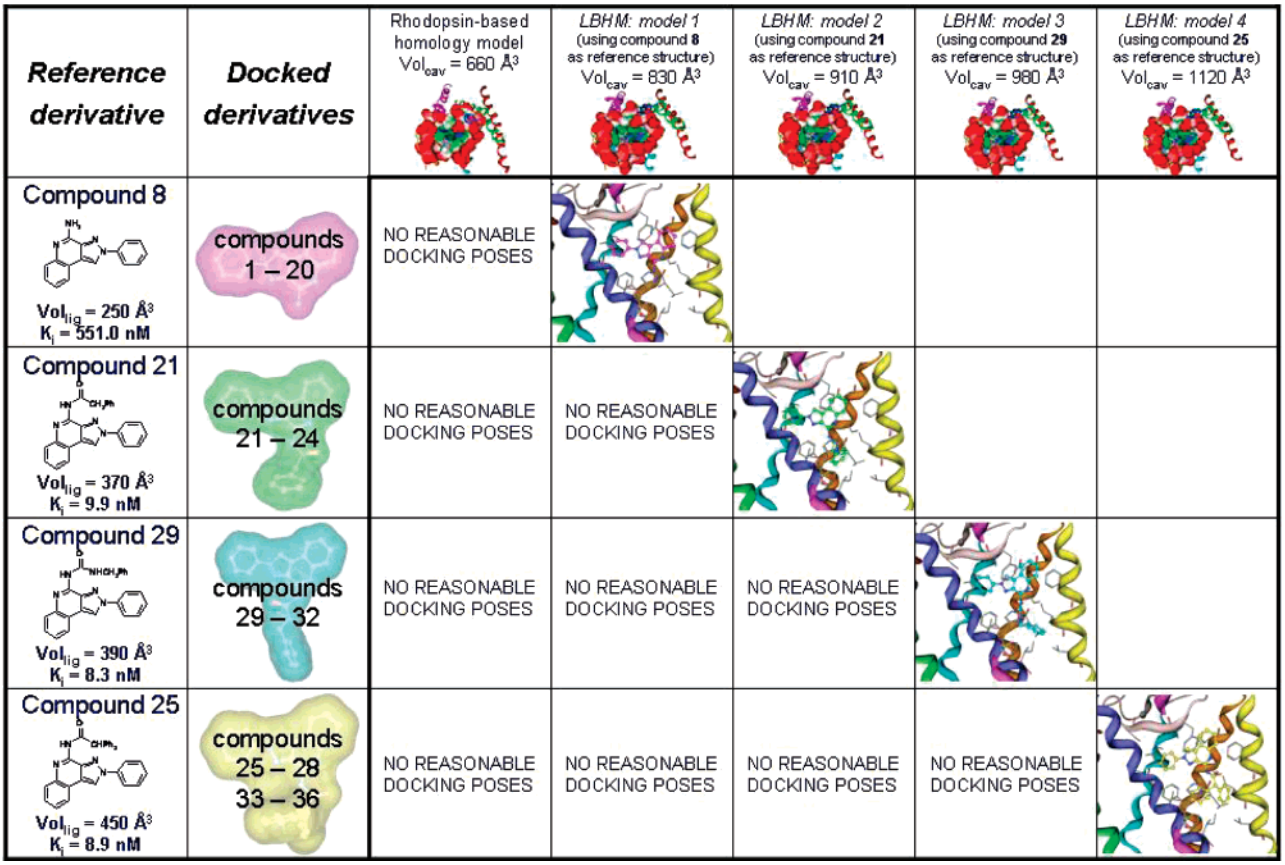

Figure 4. Ligand-based homology modeling (LBHM) data collection. Each "reference derivative" (compounds **8**, **21**, **25**, and **29**) was used as ligand template during the homology modeling process. Consequently, four different conformational states (models 1−4) were selected as putative ambassadors of the conformational changes induced by different ligand binding. Depending on their different structure topologies, all other antagonists (docked derivatives) were docked into the most complementary receptor models.

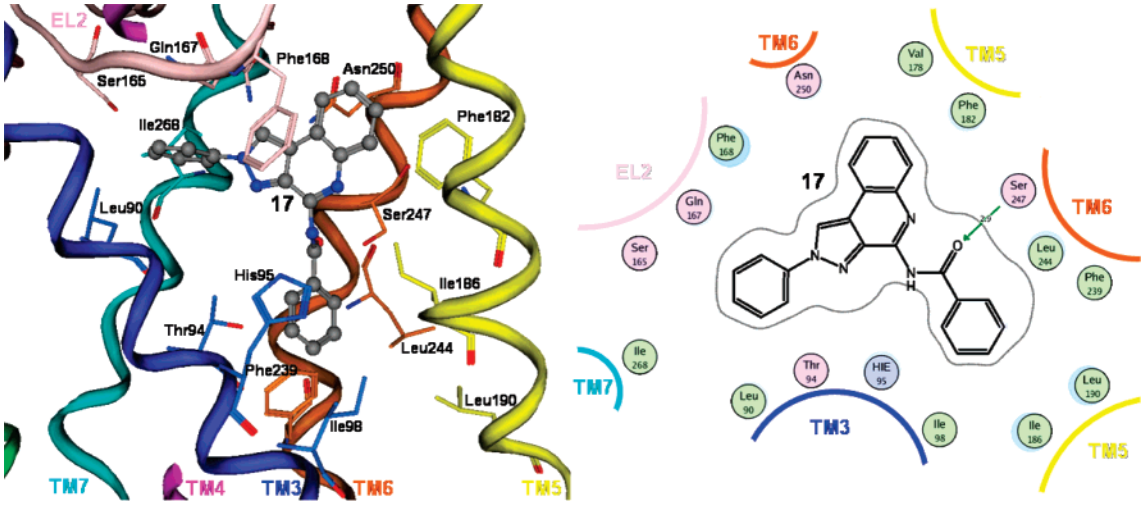

Figure 5. (Left) Hypothetical binding motif of the representative newly synthesized 2-arylpyrazolo[3,4-*c*]quinoline antagonists. The most energetically favorable docked conformation of derivative **17** is viewed from the membrane side facing TM helices 4 and 5. To clarify the TM cavity, the view of TM4 from Leu136 to Pro145 was voluntarily omitted. Side chains of some amino acids important for ligand recognition are highlighted. Hydrogen atoms are not displayed. (Right) Diagram of the binding site of a complex. Polar amino acids are coded by violet circles, hydrophobic amino acids by green circles, and side chains' donor/acceptor interactions are depicted by green arrows, where interaction strength is annotated by the distance between the two heavy atoms, in angstroms.

Trp243 (6.48), Leu244 (6.49), Leu264 (7.35), and Ile268 (7.39). However, molecular docking studies carried out for all the pyrazoloquinoline antagonists, using the appropriate conformational states of the receptor as listed in Figure 4, have shown a similar binding motif, indicating that a common receptor-driven pharmacophore model can be depicted. This finding is consistent with our previously reported studies.[22−30] Interestingly, none of the new pyrazoloquinoline antagonists found an energetically stable docking pose in the conventional RBHM-driven A_3 model. This is mainly due to the unfavorable topological complementarity among these antagonists and corresponding RBHM-driven TM binding cavity. In particular, highly destabilizing van der Waals interactions (steric conflicts) seem to be the reason for a lack of topological complementarities. These steric conflicts are drastically reduced or completely eliminated after application of the LBHM approach.

The ligand recognition occurs in the upper region of the TM bundle, and the pyrazoloquinoline moiety is surrounded by TMs 3, 5, 6, 7 with the substituent in the 4-position oriented toward the intracellular environment. As shown in Figure 5, the phenyl ring at the 2-position is close to TMs 3, 6, and 7. Interestingly, an important hydrogen-bonding network can be observed in all energetically stable docked conformations of all pyrazoloquinoline antagonists; in particular, Thr94 (3.36), His95 (3.37), and Ser247 (6.52) are able to interact through hydrogen bonding with the 4-carbonyl oxygen of compounds **1**−**7**, with the 4-amino group of compounds **8**−**12**, or with the 4-acylamino group of compounds **13**−**36**. These polar amino acids seem to be critical for the recognition of all antagonist structures and for receptor selectivity. In particular, Ser247 (6.52) of the hA_3 receptor subtype is not present in the corresponding position of A_1 and A_2 receptors, where the residue is replaced by a histidine (His251 in hA_1, His250 in hA_{2A}, and His251 in hA_{2B}). The histidine side chain is bulkier than serine and, possibly for this reason, large substituents at the 4-position of the pyrazoloquinoline framework are not well-tolerated by A_1 and A_2 receptor subtypes. Indeed, 4-acylamino and 4-benzylureido analogs (**13**−**36**) are inactive or modestly active on hA_1 and hA_{2A} ARs. On the contrary, the hydroxyl group of Ser247 (6.52) of the hA_3 receptor is appropriately positioned to form a hydrogen-bonding interaction with the carbonyl oxygen of the 4-amide/ureide group of compounds **13**−**36**. These observations support the importance of a 4-*N*-acyl/carbamoyl group in modulating receptor selectivity.

Specifically referring to 4-*N*-acylated derivatives, hA_3 receptor affinity increases with the bulkiness of the R_4 substituent (compare the 4-acetylamino compounds **13**−**16** with the 4-benzoyl compounds **17**−**20**). The hydrophobic environment of the five nonpolar amino acids, Ile98 (3.40), Ile186 (5.47), Leu190 (5.51), Phe239 (6.44), and Leu244 (6.49), can justify this affinity trend. Moreover, substituents bulkier than phenyl (compounds **21**−**36**) are also tolerated. In fact, compounds **21**−**36** maintain their hA_3 receptor affinities in the low nanomolar range (K_i < 30 nM). Both hydrogen-bonding interactions and shape/hydrophobicity complementarity of this region of the binding pocket are crucial for the anchoring of all compounds with a hydrophobic substituent at the R_4 position. Indeed, the introduction of a hydrophobic R substituent, such as a methyl group, on the 2-phenyl ring (compounds **14**, **15**, **18**, **19**, **22**, **23**, **26**, **27**, **30**, **31**, **34**, **35**) does not play any special role even if this ring is surrounded by a hydrophobic pocket delimited by Leu90 (3.32) and Ile268 (7.39).

The effect of a hydrophobic substituent at the R-position is significantly different for the 4-oxo- and 4-aminopyrazoloquinoline derivatives **1**−**12** with respect to compounds **13**−**36**. Both the 4-oxo (**1**−**7**) and 4-amino (**8**−**12**) derivatives interact only with the upper part of the binding pocket, and the introduction of a methyl group in meta or para position of the phenyl ring (compounds **2**, **3**, **9**, **10**) increases affinity versus the hA_3 receptor. The 2-(4-methoxyphenyl)pyrazoloquinoline derivatives, either 4-oxo or 4-amino substituted (compounds **4** and **11**, respectively), can favorably interact with Ser165 of the second extracellular loop (EL2). The hydroxyl group of Ser is separated by 3 Å from the *p*-methoxy group and correctly oriented to form a weak hydrogen bond. The displacement of the methoxy substituent from the para to the meta position (derivatives **5** and **12**) causes the loss of interaction with Ser165. The replacement of the 4-methoxy with a nitro group leads to unfavorable steric and dipolar interactions with Leu90 (3.32) and Ile268 (7.39) that are responsible for the reduction of affinity observed for compound **6**.

In contrast, introduction of the 4-methoxy at the R-position on the 4-acylamino/4-benzylureido derivatives does not produce considerable effects on hA_3 receptor affinity: when the bulkiness of the R_4 substituent is increased, the position of 2-phenyl shifts away from EL2 and, in particular, the hydrogen-bonding interaction with the residue of Ser165 (EL2) is lost.

Finally, the pyrazoloquinoline moiety does not present any specific hydrogen-bonding interaction with Gln167 (EL2), Phe168 (EL2), or Asn250 (6.55) as previously reported for other classes of antagonists, signifying that these interactions are ancillaries with respect to all others mentioned above.

Conclusion

The present study has led to new potent and selective hA_3 AR antagonists belonging to the class of the 2-arylpyrazolo-[3,4-*c*]quinolines. The observed structure−activity relationships are clearly rationalized by the recently published ligand-based homology modeling approach, indicating that the chemical and topological properties of the different ligands might induce important conformational changes in the antagonist-driven binding site of the hA_3 AR.

The two selected hA_3 AR antagonists **25** and **36**, tested in an in vitro rat model of cerebral ischemia, proved to be efficacious in protecting against the irreversible failure of excitatory neurotrasmission caused by oxygen and glucose deprivation in the hippocampus. In addition, compounds **25** and **36** prevented or delayed the appearance of AD, thus confirming that potent and selective A_3 AR antagonists may substantially increase the resistance of the CA1 hippocampal region to ischemic damage.

Experimental Section

(A) Chemistry. The microwave-assisted syntheses were performed using an Initiator EXP Microwave Biotage instrument (frequency of irradiation: 2.45 GHz). Silica gel plates (Merck F_{254}) and silica gel 60 (Merck, 70−230 mesh) were used for analytical and column chromatography, respectively. All melting points were determined on a Gallenkamp melting point apparatus. Microanalyses were performed with a Perkin-Elmer 260 elemental analyzer for C, H, N, and the results were within ±0.4% of the theoretical values, unless otherwise stated. The IR spectra were recorded with a Perkin-Elmer Spectrum RX I spectrometer in Nujol mulls and are expressed in cm^{-1}. The ^1H NMR spectra were obtained with a Brucker Avance 400 MHz instrument. The chemical shifts are reported in δ (ppm) and are relative to the central peak of the solvent, which was DMSO-d_6 or $CDCl_3$. The following abbreviations are used: s = singlet, d = doublet, dd = double doublet, t = triplet, m = multiplet, br = broad, and ar = aromatic protons.

General Procedure for the Synthesis of 2-Aryl-2,5-dihydro-4*H*-pyrazolo[3,4-*c*]quinolin-4-ones (1−5) and 2-Benzyl-2,5-dihydro-4*H*-pyrazolo[3,4-*c*]quinolin-4-one (7). A suspension of suitable arylhydrazine hydrochlorides (9.2 mmol) or benzylhydrazine dihydrochloride (9.2 mmol) and ethyl 2-(3-indolyl)-2-oxoethanoate[32] (4.6 mmol) in absolute ethanol (10 mL) and glacial acetic acid (5−6 drops) was irradiated at 140 °C for 3 min (derivatives **1**−**4** and **7**) or at 160 °C for 6 min (derivative **5**). The suspension was cooled at room temperature and the solid collected, washed with water, and recrystallized.

1: yield 98%; mp >300 °C (lit. mp >300 °C).[18]

2: yield 85%; mp 293−294 °C (lit. mp 291−292 °C).[18]

3: yield 95%; mp >300 °C (lit. mp >300 °C).[18]

4: yield 85%; mp 291−292 °C (lit. mp 291−292 °C).[18]

5: yield 80%; mp 280−281 °C (glacial acetic acid); ^1H NMR (DMSO-d_6) 3.90 (s, 3H, OMe), 7.05 (d, 1H, ar, J = 8.3 Hz), 7.23−7.27 (m, 1H, ar), 7.35−7.41 (m, 2H, ar), 7.53 (t, 1H, ar, J = 8.0 Hz), 7.60−7.62 (m, 2H, ar), 7.95 (d, 1H, ar, J = 7.6 Hz), 9.50 (s, 1H, H-1), 11.50 (s, 1H, NH); IR 3140, 1670. Anal. ($C_{17}H_{13}N_3O_2$) C, H, N.

7: yield 70%; mp 217−218 °C (lit. mp 215−216 °C).[18]

4-Nitrophenylhydrazone of Ethyl 2-(3-Indolyl)-2-oxoethanoate (37). An excess of 4-nitrophenylhydrazine (20 mmol) and 12 M hydrochloric acid (23 mmol, 1.9 mL) was added to a suspension of ethyl 2-(3-indolyl)-2-oxoethanoate[32] (9.2 mmol) in absolute ethanol (40 mL) and glacial acetic acid (0.8 mL). The mixture was heated at reflux for 20 h and then cooled at room temperature. The dark brown solid was collected, washed with ethanol, and recrystallized from dimethylformamide: yield 93%; mp 293−294 °C; ^1H NMR (DMSO-d_6) 1.38 (t, 3H, Me, J = 8.1 Hz), 4.48 (q, 2H, CH_2, J = 8.1 Hz), 7.20−7.25 (m, 2H, ar), 7.41 (d, 1H, ar, J = 7.9 Hz), 7.47−7.49 (m, 2H, ar), 7.74 (d, 1H, ar, J = 2.6 Hz), 8.22−8.27 (m, 3H, ar), 11.13 (s, 1H, NH), 11.60 (s, 1H, NH). Anal. ($C_{18}H_{16}N_4O_4$) C, H, N.

2,5-Dihydro-2-(4-nitrophenyl)-4*H*-pyrazolo[3,4-*c*]quinolin-4-one (6). Compound **37** was heated at about 230 °C, under nitrogen atmosphere, for 32 h and the resulting solid was recrystallized from dimethylformamide: yield 57%; mp >300 °C; ^1H NMR (DMSO-d_6) 7.26 (t, 1H, ar, J = 7.1 Hz), 7.35−7.43 (m, 2H, ar), 7.96 (d, 1H, ar, J = 7.5 Hz), 8.41 (d, 2H, ar, J = 9.0 Hz), 8.49 (d, 2H, ar, J = 9.0 Hz), 9.69 (s, 1H, H-1), 11.56 (s, 1H, NH); IR 1674, 1594, 1341. Anal. ($C_{16}H_{10}N_4O_3$) C, H, N.

4-Chloro-2-(3-methoxyphenyl)-2*H*-pyrazolo[3,4-*c*]quinoline (38). A mixture of **5** (4.8 mmol) and phosphorus pentachloride (1.4 mmol) in phosphorus oxychloride (25 mL) was heated at reflux for 2 h. Evaporation at reduced pressure of the excess of phosphorus oxychloride gave a yellow residue which was treated with cold water (50 mL) and quickly collected. The 4-chloro derivative **38** was unstable; nevertheless, it was pure enough to be characterized and used without further purification: yield 92%; ^1H NMR (DMSO-d_6) 3.92 (s, 3H, OMe), 7.13 (d, 1H, ar, J = 6.1 Hz), 7.58 (t, 1H, ar, J = 8.2 Hz), 7.69−7.76 (m, 4H, ar), 8.01 (d, 1H, ar, J = 8.0 Hz), 8.32 (d, 1H, ar, J = 7.0 Hz), 9.87 (s, 1H, H-1).

2-(3-Methoxyphenyl)-2*H*-pyrazolo[3,4-*c*]quinolin-4-amine (12). A mixture of **38** (3 mmol) in absolute ethanol saturated with ammonia was heated overnight at 120 °C in a sealed tube. The solid that precipitated upon cooling was collected, washed with water, and recrystallized from ethanol: yield 80%; mp 201−203 °C; ^1H NMR (DMSO-d_6) 3.90 (s, 3H, OMe), 6.96 (br s, 2H, NH_2), 7.03−7.05 (m, 1H, ar), 7.20−7.22 (m, 1H, ar), 7.32−7.40 (m, 1H, ar), 7.49−7.53 (m, 2H, ar), 7.63−7.70 (m, 2H, ar), 7.99 (d, 1H, ar, J = 7.9 Hz), 9.51 (s, 1H, H-1); IR 3443, 3286. Anal. ($C_{17}H_{14}N_4O$) C, H, N.

General Procedure for the Synthesis of 4-Acetylamino-2-aryl-2*H*-pyrazolo[3,4-*c*]quinolines (14−16), 2-Aryl-4-benzoylamino-2*H*-pyrazolo[3,4-*c*]quinolines (18−20), 2-Aryl-4-phenylacetylamino-2*H*-pyrazolo[3,4-*c*]quinolines (22−24), and 2-Aryl-4-diphenylacetylamino-2*H*-pyrazolo[3,4-*c*]quinolines (25−28). A mixture of the 4-amino derivatives **8**−**11** (1 mmol), the suitable carboxylic acid (6 mmol), 1-(3-(dimethylamino)propyl))-3-ethylcarbodiimide hydrochloride (6 mmol), 1-hydroxybenzotriazole (6 mmol), triethylamine (15 mmol), and 4-(dimethylamino)pyridine (0.1 mmol) in anhydrous dimethylformamide (5 mL) was stirred at room temperature for 2−5 h (compounds **18**−**20**, **22**−**24**) or for 25−27 h (derivatives **14**−**16**, **25**−**28**). The solid was collected by filtration and washed with water (about 10 mL) to yield the crude 4-amido derivatives **18**−**20**, **22**−**24**, **26**−**28**. A second crop of these compounds and the 4-acetamido and 4-diphenylacetamido derivatives **14**−**16** and **25**, respectively, were obtained by diluting with water (10 mL) the clear mother dimethylformamide solution. The crude solid was recrystallized from the suitable solvent.

14: yield 88%; mp 232−234 °C (2-ethoxyethanol); ^1H NMR (DMSO-d_6) 2.41 (s, 3H, CH_3), 2.47 (s, 3H, CH_3), 7.33 (d, 1H, ar, J = 7.6 Hz), 7.52−7.61 (m, 3H, ar), 7.86 (d, 1H, ar, J = 7.1 Hz), 7.94 (d, 1H, ar, J = 7.7 Hz), 8.00 (s, 1H, ar), 8.21 (d, 1H, ar, J = 8.1 Hz), 9.67 (s, 1H, H-1), 10.25 (s, 1H, NH); IR 3376, 1673. Anal. ($C_{19}H_{16}N_4O$) C, H, N.

15: yield 96%; mp 253−255 °C (2-ethoxyethanol); ^1H NMR (DMSO-d_6) 2.40 (s, 3H, CH_3), 2.42 (s, 3H, CH_3), 7.46 (d, 2H, ar,

J = 8.3 Hz), 7.54−7.61 (m, 2H, ar), 7.86 (d, 1H, ar, J = 7.5 Hz), 8.03 (d, 2H, ar, J = 8.3 Hz), 8.21 (d, 1H, ar, J = 8.6 Hz), 9.64 (s, 1H, H-1), 10.24 (s, 1H, NH); IR 3380, 1674. Anal. ($C_{19}H_{16}N_4O$) C, H, N.

16: yield 81%; mp 196−199 °C (2-ethoxyethanol); ^{1}H NMR (DMSO-d_6) 2.40 (s, 3H, CH_3), 3.86 (s, 3H, OCH_3), 7.19 (d, 2H, ar, J = 8.9 Hz), 7.55−7.60 (m, 2H, ar), 7.85 (d, 1H, ar, J = 7.6 Hz), 8.05 (d, 2H, ar, J = 8.8 Hz), 8.20 (d, 1H, ar, J = 7.0 Hz), 9.57 (s, 1H, H-1), 10.24 ((s, 1H, NH); IR 3252, 1670. Anal. ($C_{19}H_{16}N_4O_2$) C, H, N.

18: yield 83%; mp 219−220 °C (2-methoxyethanol); ^{1}H NMR ($CDCl_3$) 2.59 (s, 3H, CH_3), 7.43−7.75 (m, 8H, ar), 7.79 (d, 1H, ar, J = 7.4 Hz), 7.92 (s, 1H, ar), 7.97 (d, 1H, ar, J = 7.6 Hz), 8.65 (s, 2H, ar), 8.67 (s, 1H, H-1); IR 3620, 1620. Anal. ($C_{24}H_{18}N_4O$) C, H, N.

19: yield 88%; mp 163−165 °C (2-methoxyethanol); ^{1}H NMR ($CDCl_3$) 2.49 (s, 3H, CH_3), 7.32−7.60 (m, 8H, ar), 7.92 (d, 2H, ar, J = 8.1 Hz), 7.96 (s, 1H, ar, J = 7.8 Hz), 8.41−8.59 (m, 2H, ar), 8.69 (s, 1H, H-1); IR 3620, 1626. Anal. ($C_{24}H_{18}N_4O$) C, H, N.

20: yield 69%; mp 203−204 °C (2-methoxyethanol); ^{1}H NMR ($CDCl_3$) 3.93 (s, 3H, CH_3), 7.09 (d, 2H, ar, J = 8.9 Hz), 7.43−7.52 (m, 6H, ar), 7.93−7.95 (m, 3H, ar), 8.49−8.52 (m, 2H, ar), 8.62 (s, 1H, H-1); IR 3629, 1626. Anal. ($C_{24}H_{18}N_4O_2$) C, H, N.

22: yield 84%; mp 184−186 °C (ethanol); ^{1}H NMR (DMSO-d_6) 2.48 (s, 3H, CH_3), 4.06 (s, 2H, CH_2), 7.26−7.61 (m, 9H, ar), 7.87 (d, 1H, ar, J = 6.9 Hz), 7.92 (d, 1H, ar, J = 7.9 Hz), 7.98 (s, 1H, ar), 8.19−8.23 (m, 1H, ar), 9.68 (s, 1H, H-1), 10.55 (s, 1H, NH); IR 3366, 1673. Anal. ($C_{25}H_{20}N_4O$) C, H, N.

23: yield 80%; mp 170−172 °C (2-methoxyethanol); ^{1}H NMR (DMSO-d_6) 2.42 (s, 3H, CH_3), 4.04 (s, 2H, CH_2), 7.26−7.29 (m, 1H, ar), 7.36 (t, 2H, ar, J = 7.5 Hz), 7.44−7.48 (m, 4H, ar), 7.57−7.59 (m, 2H, ar), 7.87 (d, 1H, ar, J = 8.8 Hz), 8.02 (d, 2H, ar, J = 8.3 Hz), 8.22 (d, 1H, ar, J = 6.5 Hz), 9.66 (s, 1H, H-1), 10.55 (s, 1H, NH); IR 3372, 1678. Anal. ($C_{25}H_{20}N_4O$) C, H, N.

24: yield 87%; mp 185−187 °C (2-ethoxyethanol); ^{1}H NMR (DMSO-d_6) 3.87 (s, 3H, CH_3), 4.05 (s, 2H, CH_2), 7.21 (d, 2H, ar, J = 9.0 Hz), 7.29 (m, 1H, ar), 7.36 (t, 2H, ar, J = 7.4 Hz), 7.45 (d, 2H, ar, J = 7.3 Hz), 7.55−7.61 (m, 2H, ar), 7.88−7.86 (m, 1H, ar), 8.04 (d, 2H, ar, J = 8.9 Hz), 8.20−8.22 (m, 1H, ar), 9.59 (s, 1H, H-1), 10.53 (s, 1H, NH); IR 3371, 1667. Anal. ($C_{25}H_{20}N_4O_2$) C, H, N.

25: yield 44%; mp 208−210 °C (2-ethoxyethanol); ^{1}H NMR (DMSO-d_6) 5.74 (br s, 1H, CH), 7.27−7.40 (m, 6H, ar), 7.49−7.71 (m, 7H, ar), 7.69 (t, 2H, ar, J = 7.7 Hz), 7.88−7.90 (m, 1H, ar), 8.13 (d, 2H, ar, J = 8.0 Hz), 8.23−8.25 (m, 1H, ar), 9.71 (s, 1H, H-9), 10.91 (s, 1H, NH); IR 3278, 1667. Anal. ($C_{30}H_{22}N_4O$) C, H, N.

26: yield 80%; mp 220−221 °C (2-ethoxyethanol); ^{1}H NMR (DMSO-d_6) 2.46 (s, 3H, CH_3), 5.75 (br s, 1H, CH), 7.27−7.40 (m, 7H, ar), 7.49−7.61 (m, 7H, ar), 7.88−7.94 (m, 2H,ar), 7.97 (s, 1H, ar), 8.23−8.24 (m, 1H, ar), 9.69 (s, 1H, H-9), 10.89 (s, 1H, NH); IR 3367, 1700. Anal. ($C_{31}H_{24}N_4O$) C, H, N.

27: yield 44%; mp 215−218 °C (2-ethoxyethanol); ^{1}H NMR (DMSO-d_6) 2.43 (s, 3H, CH_3), 5.72 (br s, 1H, CH), 7.27−7.31 (m, 2H, ar), 7.38 (t, 4H, ar, J = 7.6 Hz), 7.49 (d, 6H, ar, J = 7.8 Hz), 7.57−7.62 (m, 2H, ar), 7.87−7.90 (m, 1H, ar), 8.02 (d, 2H, ar, J = 8.0 Hz), 8.21−8.23 (m, 1H, ar), 9.67 (s, 1H, H-9), 10.94 (br s, 1H, NH); IR 3284, 1681. Anal. ($C_{31}H_{24}N_4O$) C, H, N.

28: yield 70%; mp 211−213 °C (2-ethoxyethanol); ^{1}H NMR (DMSO-d_6) 3.88 (s, 3H, CH_3), 5.74 (br s, 1H, CH), 7.17−7.14 (m, 8H, ar), 7.49 (d, 4H, ar, J = 7.4 Hz), 7.56−7.62 (m, 2H, ar), 7.87−7.90 (m, 1H, ar), 8.02 (d, 2H, ar, J = 9 Hz), 8.21−8.24 (m, 1H, ar), 9.60 (s, 1H, H-9), 10.89 (s, 1H, NH); IR 3318, 1675. Anal. ($C_{31}H_{24}N_4O_2$) C, H, N.

General Procedure for the Synthesis of 4-Benzylureido-2-aryl-2*H*-pyrazolo[3,4-*c*]quinolines (30−32). Benzyl isocyanate (1.5 mmol) was added to a suspension of the 4-amino derivatives **9**−**11** (1 mmol) in anhydrous tetrahydrofuran (20 mL). The mixture was refluxed for 24−48 h under nitrogen atmosphere. The resulting solid was collected, washed with diethyl ether, and recrystallized.

30: yield 95%; mp 226−228 °C (ethanol); ^{1}H NMR (DMSO-d_6) 2.32 (s, 3H, CH_3), 4.60 (d, 2H, CH_2, J = 5.5 Hz), 7.28−7.52 (m, 9H, ar), 7.77 (d, 1H, J = 8.1 Hz), 8.03 (s, 1H, ar), 8.14 (d, 2H, 7.1 Hz), 9.27 (s, 1H, NH), 9.67 (s, 1H, H-9), 10.50 (t, 1H, NH, J = 5.5 Hz); IR 3420, 1686. Anal. ($C_{25}H_{21}N_5O$) C, H, N.

31: yield 68%; mp 224−226 °C (2-methoxyethanol); ^{1}H NMR (DMSO-d_6) 2. 41(s, 3H, CH_3), 4.61 (d, 2H, CH_2, J = 5.7 Hz), 7.29−7.51 (m, 9H, ar), 7.77 (d, 1H, ar, J = 7.7 Hz), 8.08−8.15 (m, 3H, ar), 9.24 (s, 1H, NH), 9.65 (s, 1H, H-9), 10.50 (t, 1H, NH, J = 5.7 Hz); IR 3423, 1687. Anal. ($C_{25}H_{21}N_5O$) C, H, N.

32: yield 78%; mp 245−246 °C (2-methoxyethanol); ^{1}H NMR (DMSO-d_6) 3.87 (s, 3H, CH_3), 4.61 (d, 2H, CH_2, J = 5.7 Hz), 7.20 (d, 1H, ar, J = 9.1 Hz), 7.27−7.55 (m, 8H, ar), 7.77 (d, 1H, ar, J = 8.3 Hz), 8.14 (m, 3H, ar), 9.18 (s, 1H, NH), 9.58 (s, 1H, H-9), 10.50 (t, 1H, NH, J = 5.7 Hz); IR 3419, 1687. Anal. ($C_{25}H_{21}N_5O_2$) C, H, N.

General Procedure for the Synthesis of 4-Dibenzoylamino-2-aryl-2*H*-pyrazolo[3,4-*c*]quinolines (33−36). A solution of benzoyl chloride (5 mmol) in anhydrous methylene chloride (3 mL) was dropwise added to a suspension of the 4-amino derivatives **8**−**11** (2.5 mmol) in anhydrous methylene chloride (7 mL) and anhydrous pyridine (25 mmol). The mixture was stirred at room temperature for about 24 h. Evaporation of the solvent at reduced pressure afforded a residue that was treated with water (4−5 mL), collected by filtration, and recrystallized.

33: yield 72%; mp 224−226 °C (2-ethoxyethanol); ^{1}H NMR (DMSO-d_6) 7.44−7.69 (m, 11H, ar), 7.78 (d, 1H, ar, J = 7.7 Hz), 7.88 (d, 4H, ar, J = 7.3 Hz), 8.02 (d, 2H, ar, J = 7.8 Hz), 8.29 (d, 1H, ar, J = 7.7 Hz), 9.81 (s, 1H, H-1); IR 1689. Anal. ($C_{30}H_{20}N_4O_2$) C, H, N.

34: yield 77%; mp 207−208 °C (ethanol); ^{1}H NMR (DMSO-d_6) 2.42 (s, 3H, CH_3), 7.31 (d, 1H, ar, J = 7.0 Hz), 7.44−7.56 (m, 8H, ar), 7.68 (t, 1H, ar, J = 7.1 Hz), 7.76−7.88 (m, 7H, ar), 8.28 (d, 1H, ar, J = 7.8 Hz), 9.77 (s, 1H, H-1); IR 1707, 1687. Anal. ($C_{31}H_{22}N_4O_2$) C, H, N.

35: yield 65%; mp 241−243 °C (2-methoxyethanol); ^{1}H NMR (DMSO-d_6) 2.33 (s, 3H, CH_3), 7.42−7.47 (m, 6H, ar), 759−7.53 (m, 3H, ar), 7.67 (t, 1H, ar, J = 7.6 Hz), 7.77 (d, 1H, ar, J = 8.3 Hz), 7.86−7.91 (m, 6H, ar), 8.28 (d, 1H, ar, J = 7.6 Hz), 9.74 (s, 1H, H-9); IR 1706, 1684. Anal. ($C_{31}H_{22}N_4O_2$) C, H, N.

36: yield 68%; mp 247−250 °C (2-methoxyethanol); ^{1}H NMR (DMSO-d_6) 3.84 (s, 3H, CH_3), 7.17 (d, 2H, ar, J = 9.0 Hz), 7.45 (t, 4H, ar, J = 7.7 Hz), 7.53−7.59 (m, 3H, ar), 7.67 (t, 1H, ar, J = 7.52 Hz), 7.77 (d, 1H, J = 7.7 Hz), 7.87 (d, 4H, ar, J = 8.2 Hz), 7.93 (d, 2H, ar, J = 7.6 Hz), 8.26 (d, 1H, J = 7.7 Hz), 9.68 (s, 1H, H-1); IR 1706, 1683. Anal. ($C_{31}H_{22}N_4O_3$) C, H, N.

(B) Biochemistry. Human A_1, A_{2A}, and A_3 Receptor Binding. Displacement of [^{3}H]DPCPX and [^{3}H]NECA from, respectively, hA_1 and hA_{2A} ARs, stably expressed in CHO cells, was performed as previously described.[43] Displacement of [^{125}I]AB-MECA from hA_3 ARs, stably expressed in CHO cells, was performed as reported in ref 20.

Rat A_1 and A_{2A} Receptor Binding. Rat brain cortex and striatum were dissected from male Wistar rats. Membrane preparation was carried out as previosly reported for the bovine membrane preparation.[44] The A_1 binding assays were performed in triplicate by incubating aliquots of brain cortex membranes (40−50 μg of protein) at 25 °C for 180 min in 0.5 mL of binding buffer (50 mM Tris/HCl, 2 mM $MgCl_2$ pH = 7.7) containing 0.2−0.5 nM [^{3}H]-DPCPX. Nonspecific binding was defined in presence of 20 μM R-PIA. Incubation was terminated by rapid filtration through Whatman GF/C glass microfiber filters and washing twice with 4 mL of ice-cold buffer. K_D value on brain cortex was 0.51 nM.[45] Binding assays at the rA_{2A} AR were performed as previously described.[44]

Rat A_3 Receptor Binding. Binding of [^{3}H]-(R)-PIA (37 Ci/mmol) to rat testis membranes was measured in the presence of DPCPX (150 nM) as previously described.[46,47] Briefly, fresh testicular tissue from Wistar rats was dissected free of epididymis, and membranes were prepared as described.[46] Rat testis membranes (0.1−0.2 mg of protein) and [^{3}H]-(R)-PIA 4 nM were incubated in

0.5 mL total volume of 50 mM Tris/HCl (pH 7.4), 1 mM EDTA, 10 mM $MgCl_2$ buffer in the presence of 150 nM DPCPX to block A_1 adenosine receptors. Nonspecific binding was determined in the presence of 15 μM (R)-PIA. Binding reactions were terminated by filtration through Whatman GF/filters under reduced pressure. Filters were washed three times with 5 mL of ice-cold buffer and introduced into scintillation vials. The radioactivity was counted in 4 mL of scintillation cocktail in a scintillation counter.

Measurement of cAMP Levels on CHO Cells Transfected with Human A_3 AR. Intracellular cAMP levels were measured using a competitive protein binding method.[48] CHO cells (~60 000), stably expressing hA_3 ARs, were plated in 24-well plates. After 48 h, the medium was removed, and the cells were incubated at 37 °C for 15 min with 0.5 mL of DMEM in the presence of Ro 20-1724 [4-(3-butoxy-4-methoxybenzyl)imidazolidin-2-one] (20 μM) and adenosine deaminase (1 U/mL). A 1 mM stock solution of the tested compound was prepared in DMSO, and subsequent dilutions were accomplished in distilled water. The effect of examined compounds at different concentrations in the presence of 100 nM NECA and 10 μM forskolin was evaluted for 15 min at 37 °C. The reaction was terminated by removing the medium and adding 0.4 N HCl. After 30 min the lysate was neutralized with KOH 4 N and the suspension was centrifuged at 800*g* for 5 min. To determine cyclic AMP production, the binding protein, prepared from beef adrenal glands, was incubated with [^{3}H]cAMP (2 nM) in distilled water and 50 μL of cell lysate or standard cAMP (0−16 pmol) at 4 °C for 150 min in a total volume of 300 μL. Bound radioactivity was separated by rapid filtration through GF/C glass fiber filters and washed twice with 4 mL of 50 mM Tris/HCl, pH 7.4. The radioactivity was measured by liquid scintillation spectrometry.

Data Analysis. The concentration of the tested compounds that produced 50% inhibition of specific [^{3}H]DPCPX, [^{3}H]NECA, and [^{125}I]AB-MECA binding (IC_{50}) was calculated using a nonlinear regression method implemented by the InPlot program (Graph-Pad, San Diego, CA) with five concentrations of displacer, each performed in triplicate. Inhibition constants (K_i) were calculated according to the Cheng−Prusoff equation.[49] The dissociation constant K_d values of [^{3}H]DPCPX, [^{3}H]NECA, and [^{125}I]AB-MECA in hA_1, hA_{2A}, and hA_3 ARs in CHO cell membranes were 3, 30, and 1.4 nM, respectively. EC_{50} values obtained in cAMP assays were calculated by nonlinear regression analysis using the equation for a sigmoid concentration−response curve (Graph-Pad, San Diego, CA).

(C) Electrophysiological Assays. Slice Preparation. All animal procedures were carried out according to the European Community Guidelines for Animal Care, DL 116/92, application of the European Communities Council Directive (86/609/EEC). Experiments were carried out on rat hippocampal slices, prepared as previously described.[50] Male Wistar rats (Harlan Italy; Udine, Italy, 150−200 g body weight) were killed with a guillotine under anesthesia with ether and their hippocampi were rapidly removed and placed in ice-cold oxygenated (95% O_2−5% CO_2) aCSF of the following composition (mM): NaCl 124, KCl 3.33, KH_2PO_4 1.25, $MgSO_4$ 2, $CaCl_2$ 2, $NaHCO_3$ 25, and D-glucose 10. Slices (400 μm thick) were cut using a McIlwain tissue chopper (The Mickle Lab. Engineering, Co. Ltd., Gomshall, U.K.) and kept in oxygenated aCSF for at least 1 h at room temperature. A single slice was then placed on a nylon mesh, completely submerged in a small chamber (0.8 mL), and superfused with oxygenated aCSF (30−32 °C) at a constant flow rate of 2 mL min^{-1}. The treated solutions reached the preparation in 90 s and this delay was taken into account in our calculations.

Extracellular Recording. Test pulses (80 μs, 0.066 Hz) were delivered through a bipolar nichrome electrode positioned in the stratum radiatum. Evoked extracellular potentials were recorded with glass microelectrodes (2−10 MΩ, Clark Electromedical Instruments, Panghourne, U.K.) filled with 150 mM NaCl, placed in the CA1 region of the stratum radiatum. Responses were amplified (BM 622, Mangoni, Pisa, Italy), digitized (sample rate, 33.33 kHz), and stored for later analysis using LTP (version 2.30D) software facilities.[51] Stimulus−response curves were obtained by gradual increases in stimulus strength at the beginning of each experiment, until a stable baseline of evoked response was reached. The test stimulus pulse was then adjusted to produce a fepsp whose slope and amplitude was 40−50% of the maximum and were kept constant throughout the experiment. The fepsp amplitude was routinely measured and expressed as the percentage of the average amplitude of the potentials measured during the 5 min preceding exposure of the hippocampal slices to OGD.

In a group of slices, simultaneously with fepsp amplitude, we also recorded AD as negative shifts in the dc mode induced by 7 min OGD.

Application of Drugs and Oxygen and Glucose Deprivation. OGD was obtained by perfusing the slice for 7 min with aCSF without glucose and gassed with nitrogen (95% N_2−5% CO_2).[52] This caused a drop in p_{O_2} in the recording chamber from about 500 mmHg (normoxia) to a range of 120−150 mmHg (after 2 min OGD) and of 35−75 mmHg (after 7 min of OGD)[50] measured with an ISO2 and its associated OXEL-1 probe (WPI, Aston, U.K.). At the end of the ischemic period, the slice was again superfused with normal, glucose-containing, oxygenated aCSF.

The selective A_3 adenosine receptor antagonists were applied for 10 min before, during, and 5 min after the ischemic episode. Concentrations of the selective adenosine A_3 receptor antagonists were chosen on the basis of K_i values on human A_3 receptors.

In a typical experimental day, a control slice was submitted to 7 min of OGD. If the recovery of fepsp amplitude after 15 min of reperfusion with glucose-containing and normally oxygenated aCSF was ≤15% of the preischemic value, a second slice from the same rat was submitted to a 7-min OGD insult in the presence of the A_3 antagonists under investigation. To confirm the result obtained in the treated group, a third slice was taken from the same rat and another 7-min OGD was performed under control conditions to verify that no difference between slices was caused by the time gap between the experiments.

Statistical Analysis. Data were analyzed using Prism 3.02 software (Graphpad Software, San Diego, CA). All numerical data are expressed as the mean ± SEM. Data were tested for statistical significance by analysis of variance (one-way ANOVA). When significant differences were observed, the Newman−Keuls multiple comparison test (one-way ANOVA) was inferred. A value of $P < 0.05$ was considered significant.

(D) Computational Methodologies. All modeling studies were carried out on a 10 CPU (PIV-3.0 GHZ and AMD64) Linux cluster running under openMosix architecture.[53]

Homology modeling, energy calculation, and docking studies were performed using the Molecular Operating Environment (MOE, version 2005.06) suite.[54]

All docked structures were fully optimized without geometry constraints using RHF/AM1 semiempirical calculations. Vibrational frequency analysis was used to characterize the minima stationary points (zero imaginary frequencies). The software package MOPAC (ver. 7),[55] implemented in MOE suite was utilized for all quantum mechanical calculations.

Homology Model of the hA_3 AR. On the basis of the assumption that GPCRs share similar TM boundaries and overall topology, a homology model of the hA_3 receptor was constructed. First, the amino acid sequences of TM helices of the A_3 receptor were aligned with those of bovine rhodopsin, guided by the highly conserved amino acid residues, including the DRY motif (D3.49, R3.50, and Y3.51) and three proline residues (P4.60, P6.50, and P7.50) in the TM segments of GPCRs. The same boundaries were applied for the TM helices of the A_3 receptor, as they were identified from the X-ray crystal structure for the corresponding sequences of bovine rhodopsin,[56] the C_R coordinates of which were used to construct the seven TM helices for the hA_3 receptor. The loop domains of the hA_3 receptor were constructed by the loop search method implemented in MOE. In particular, loops are modeled first in random order. For each loop, a contact energy function analyzes the list of candidates collected in the segment searching stage, taking into account all atoms already modeled and any atoms specified by the user as belonging to the model environment. These energies

are then used to make a Boltzmann-weighted choice from the candidates, the coordinates of which are then copied to the model. Any missing side chain atoms are modeled using the same procedure. Side chains belonging to residues whose backbone coordinates were copied from a template are modeled first, followed by side chains of modeled loops. Outgaps and their side chains are modeled last. Special caution has to be given to the second extracellular loop (EL2), which has been described in bovine rhodopsin as folding back over transmembrane helices[56] and, therefore, limiting the size of the active site. Hence, amino acids of this loop could be involved in direct interactions with the ligands. A driving force to this peculiar fold of the EL2 loop might be the presence of a disulfide bridge between cysteines in TM3 and EL2. Since this covalent link is conserved in all receptors modeled in the current study, the EL2 loop was modeled using a rhodopsin-like constrained geometry around the EL2−TM3 disulfide bridge. After the heavy atoms were modeled, all hydrogen atoms were added, and the protein coordinates were then minimized with MOE using the AMBER94 force field.[57] The minimizations were carried out by the 1000 steps of steepest descent followed by conjugate gradient minimization until the rms gradient of the potential energy was less than 0.1 kcal mol^{-1} $Å^{-1}$. Protein stereochemistry evaluation was performed by several tools (Ramachandran and χ plots measure φ/ψ and $\chi1/\chi2$ angles, clash contacts reports) implemented in MOE suite.[54]

Ligand-Based Homology Modeling. We have recently revisited the rhodopsin-based model of the human A_3 receptor in its resting state (antagonist-like state), taking into account a novel strategy to simulate the possible receptor reorganization induce by the antagonist binding.[30] We called this new strategy *ligand-based homology modeling*. Briefly, ligand-based homology modeling technique is an evolution of a conventional homology modeling strategy that combined the Boltzmann-weighted randomized modeling procedure adapted from Levitt[58] with a specialized algorithm for the proper handling of insertions and deletions of any selected extra atoms during the energy tests and minimization stages of the modeling procedure.[54] The ligand-based homology modeling option is very useful when one wishes to build a homology model in the presence of a ligand docked to the primary template or other proteins known to be complexed with the sequence to be modeled.[54] In this specific case both model building and refinement take into account the presence of the ligand in terms of specific steric and chemical features. In order to generate a initial ensemble of ligand poses, a conventional docking procedure (see next section for details) with reduced van der Waals radii (equal to 75%) and an increased Coulomb-vdW cutoff (cutoff on 10 Å; cutoff on 12 Å) was performed. For each pose, a homology model is then generated to accommodate the ligand by reorienting nearby side chains. These residues and the ligand are then locally minimized. Finally, each ligand is redocked into its corresponding low-energy protein structures and the resulting complexes are ranked according to MOEScore.[54]

Different quantitative measurements of molecular volume of the receptor binding cavities were carried out using MOE suite.[54] Prediction of antagonist−receptor complex stability (in terms of corresponding pK_i value) and the quantitative analysis for non-bonded intermolecular interactions (H-bonds, transition metal, water bridges, hydrophobic) were calculated and visualized using several tools implemented in MOE suite.[54]

Molecular Docking of the hA_3 AR Antagonists. All antagonist structures were docked into the hypothetical TM binding site by using the MOE-dock tool, part of the MOE suite. Searching is conducted within a user-specified 3D docking box (the standard protocol selects all atoms inside 12 Å from the center of mass of the binding cavity), using the Tabu Search[59] protocol (standard parameters are: 1000 steps/run, 10 attempts/step, and 10 Tabu list length) and the MMFF94 force field.[60] MOE-Dock performs a user-specified number of independent docking runs (50 in our specific case) and writes the resulting conformations and their energies in a molecular database file. The resulting docked complexes were subjected to MMFF94 energy minimization until the rms of conjugate gradient was <0.1 kcal mol^{-1} $Å^{-1}$. Charges for the ligands were imported from the MOPAC output files. To better refine all antagonist−receptor complexes, a rotamer exploration of all side chains involved in the antagonist binding was carried out. Rotamer exploration methodology was implemented in the MOE suite.[54]

Acknowledgment. This work was supported by a grant of the Italian Ministry for University and Research (MIUR, FIRB RBNE03YA3L project). The molecular modeling work coordinated by S.M. was carried out with financial support from the University of Padova, Italy, and the Italian Ministry for University and Research (MIUR), Rome, Italy. The electrophysiological work was supported by a grant of the Italian Ministry for University and Research (MIUR) and by Ente Cassa di Risparmio di Firenze (2004/0747). We thank Dr. Karl-Norbert Klotz of the University of Wüzburg, Germany, for providing cloned hA_1, hA_{2A} and hA_3 receptors expressed in CHO cells. S.M. is also very grateful to Chemical Computing Group for the scientific and technical partnership.

Supporting Information Available: Combustion analysis data of the newly synthesized compounds. This material is available free of charge via the Internet at http://pubs.acs.org.

References

(1) Fredholm, B. B.; Ijzerman, A. P.; Jacobson, K. A.; Klotz, K. N.; Linden, J. International union of Pharmacology XXV. Nomenclature and classification of adenosine receptors. *Pharmacol. Rev*. **2001**, *53*, 527−552.

(2) Jacobson, K. A.; Knutsen, L. J. S. P1 and P2 purine and pyrimidine receptor ligands. In *Purinergic and Pyrimidinergic Signalling*; Abbracchio, M. P., Williams, M., Eds.; Handbook of Experimental Pharmacology; Springer: Berlin, 2001; Vol. 151/1; pp 129−175.

(3) Abbracchio, M. P.; Brambilla, R.; Kim, H. O.; von Lubitz, D. K. J. E.; Jacobson, K. A.; Cattabeni, F. G-protein-dependent activation of phospholipase-C by adenosine A_3 receptor in rat brain. *Mol. Pharmacol*. **1995**, *48*, 1083−1045.

(4) Ali, H.; Choi, O. H.; Fraundorfer, P. F.; Yamada, K.; Gonzaga, H. M. S.; Beaven, M. A. Sustained activation of phospholipase-D via adenosine A_3 receptors is associated with enhancement of antigen-ionophore-induced and Ca^{2+}-ionophore-induced secretion in a rat mast-cell line. *J. Pharmacol. Exp. Ther*. **1996**, *276*, 837−845.

(5) Shneyvays, V.; Leshem, D.; Zinman, T.; Mamedova, L. K.; Jacobson, K. A.; Shainberg, A. Role of adenosine A_1 and A_3 receptors in regulation of cardiomyocyte homeostasis after mitochondrial respiratory chain injury. *Am. J. Physiol. Heart Circ. Physiol.* **2005**, *288*, H2792−H2801.

(6) Englert, M.; Quitterer, U.; Klotz, K. N. Effector coupling of stably tranfected human A_3 adenosine receptor in CHO cells. *Biochem. Pharmacol*. **2002**, *64*, 61−65.

(7) Jacobson, K. A.; Gao, Z.-G. Adenosine receptors as therapeutic targets. *Nat. Rev. Drug Discovery* **2006**, *5*, 247−264.

(8) Ribeiro, J. A.; Sebastião, A. M.; de Mendonça, A. Adenosine receptors in the nervous system: Pathophysiological implications. *Prog. Neurobiol*. **2003**, *68*, 377−392.

(9) Wilcox, C. S.; Welch, W. J.; Schreiner, G. F.; Belardinelli, L. Natriuretic and diuretic actions of a highly selective adenosine receptor antagonist. *J. Am. Soc. Nephrol*. **1999**, *10*, 714−720.

(10) Gottlieb, S. S.; Skettino, S. L.; Wolff, A.; Beckman, E.; Fisher, M. L.; Freudenberger, R.; Gladwell, T.; Marshall, J.; Cines, M.; Bennet, D.; Liittschwager, E. B. Effects of BG9719 (CVT-124), an A_1 adenosine receptor antagonist, and Furosemide on glomerular filtration rate and natriuresis in patients with congestive heart failure. *J. Am. Coll. Cardiol*. **2000**, *35*, 56−59.

(11) de Mendonça, A.; Sebastião, A. M.; Ribeiro, J. A. Adenosine: Does it have a neuroprotective role after all? *Brain Res. Rev.* **2000**, *33*, 258−274.

(12) Maemoto, T.; Tada, M.; Mihara, T.; Ueyama, N.; Matsuoka, H.; Harada, K.; Yamaji, T.; Shirakawa, J.; Kuroda, S.; Akahane, A.; Iwashita, A.; Matsuoka, N.; Mutoh, S. Pharmacological characterization of FR194921, a new potent, selective, and orally active antagonist for the central adenosine A_1 receptor. *J. Pharmacol. Sci*. **2004**, *96*, 42−52.

(13) Lee, H. T.; Ota-Setlik, A.; Xu, H.; D'Agati, V. D.; Jacobson, M. A.; Emala, C. W. A_3 adenosine receptor knockout mice are protected against ischemia- and myoglobinuria-induced renal failure. *Am. J. Physiol. Renal. Physiol* **2003**, *284*, 267−273.

(14) Brambilla, R.; Cattabeni, F.; Ceruti, S.; Barbieri, D.; Franceschi C.; Kim, Y-C; Jacobson, K. A.; Klotz, K.-N; Lohse, M. J.; Abbracchio, M. P.; Activation of the A_3 adenosine receptor affect cell cycle progression and cell growth. *Naunyn-Schmiedeberg's Arch. Pharmacol.* **2000**, *361*, 225−234.
(15) Pugliese, A. M.; Coppi, E.; Spalluto, G.; Corradetti, R.; Pedata, F. A_3 adenosine receptor antagonists delay irreversible synaptic failure caused by oxygen and glucose deprivation in the rat CA1 hippocampus in vitro. *Br. J. Pharmacol.* **2006**, *147*, 524−532.
(16) Merighi, S.; Mirandola, P.; Varani, K.; Gessi, S.; Leung, E.; Baraldi, P. G.; Tabrizi, M. A.; Borea, P. A. A glance at adenosine receptors: A novel target for antitumor therapy. *Pharmacol. Therapeut.* **2003**, *100*, 31−48.
(17) Merighi, S.; Benini, A.; Mirandola, P.; Gessi, S.; Varani, K.; Leung, E.; Maclennan, S.; Borea, P. A. Adenosine modulates vascular endotelial growth factor expression via hypoxia-inducible factor-1 in human glioblastoma cells. *Biochem. Pharmacol.* **2006**, *72*, 19−31.
(18) Colotta, V.; Catarzi, D.; Varano, F.; Cecchi, L.; Filacchioni, G.; Martini, C.; Trincavelli, L.; Lucacchini, A. Synthesis and structure-activity relationships of a new sets of 2-arylpyrazolo[3,4-*c*]quinoline derivatives as adenosine receptor antagonists. *J. Med. Chem.* **2000**, *43*, 3118−3124.
(19) Colotta, V.; Catarzi, D.; Varano, F.; Cecchi, L.; Filacchioni, G.; Martini, C.; Trincavelli, L.; Lucacchini, A. 1,2,4-Triazolo[4,3-*a*]-quinoxalin-1-one: A versatile tool for the synthesis of potent and selective adenosine receptor antagonists. *J. Med. Chem.* **2000**, *43*, 1158−1164.
(20) Colotta, V.; Catarzi, D.; Varano, F.; Filacchioni, G.; Martini, C.; Trincavelli, L.; Lucacchini, A. Synthesis and structure−activity relationships of a new set of 1,2,4-triazolo[4,3-*a*] quinoxalin-1-one derivatives as adenosine receptor antagonists. *Bioorg. Med. Chem.* **2003**, *11*, 3541−3550.
(21) Colotta, V.; Catarzi, D.; Varano, F.; Filacchioni, G.; Martini, C.; Trincavelli, L.; Lucacchini, A. Synthesis of 4-amino-6-(hetero)-arylalkylamino-1,2,4-triazolo[4,3-*a*] quinoxalin-1-one derivatives as potent A_{2A} adenosine receptor antagonists. *Bioorg. Med. Chem.* **2003**, *11*, 5509−5518.
(22) Colotta, V.; Catarzi, D.; Varano, F.; Calabri, F. R.; Lenzi, O.; Filacchioni, G.; Trincavelli, L.; Martini, C.; Deflorian, F.; Moro, S. 1,2,4-Triazolo[4,3-*a*]quinoxalin-1-one moiety as an attractive scaffold to develop new potent and selective human A_3 adenosine receptor antagonists: Synthesis, pharmacological and ligand-receptor modeling studies. *J. Med. Chem.* **2004**, *47*, 3580−3590.
(23) Catarzi, D.; Colotta, V.; Varano, F.; Calabri, F. R.; Lenzi, O.; Filacchioni, G.; Trincavelli, L.; Martini, C.; Tralli, A.; Montopoli, C.; Moro, S. 2-Aryl-8-chloro-1,2,4-triazolo[1,5-*a*]quinoxalin-4-amines as highly potent A_1 and A_3 adenosine receptor antagonists. *Bioorg. Med. Chem.* **2005**, *13*, 705−715.
(24) Catarzi, D.; Colotta, V.; Varano, F.; Lenzi, O.; Filacchioni, G.; Trincavelli, L.; Martini, C.; Montopoli, C.; Moro, S. 1,2,4-Triazolo-[1,5-*a*]quinoxaline as a versatile tool for the design of selective human A_3 adenosine receptor antagonists: Synthesis, biological evaluation and molecular modeling studies of 2-(hetero)aryl- and 2-carboxy-substituted derivatives. *J. Med. Chem.* **2005**, *48*, 7932−7945.
(25) Lenzi, O.; Colotta, V.; Catarzi, D.; Varano, F.; Filacchioni, G.; Martini, C.; Trincavelli, L.; Ciampi, O.; Marighetti, F.; Morizzo, E.; Moro, S. 4-Amido-2-aryl-1,2,4-triazolo[4,3-*a*]quinoxalin-1-ones as new potent and selective human A_3 adenosine receptor antagonists. Synthesis, pharmacological evaluation and and ligand-receptor modeling studies. *J. Med. Chem.* **2006**, *49*, 3916−3925.
(26) Moro, S.; Deflorian, F.; Spalluto, G.; Pastorin, G.; Cacciari, B. et al. Demystifying the three dimensional structure of G protein-coupled receptors (GPCRs) with the aid of molecular modeling. *Chem. Commun.* (*Camb.*) **2003**, *24*, 2949−2956.
(27) Moro, S.; Spalluto, G.; Jacobson, K. A. Techniques: Recent developments in computer-aided engineering of GPCR ligands using the human A_3 adenosine receptor as an example. *Trends Pharmacol. Sci.* **2005**, *26*, 44−51.
(28) Moro, S.; Deflorian, F.; Bacilieri, M.; Spalluto, G. Novel strategies for the design of new potent and selective human A_3 receptor antagonists: An update. *Curr. Med. Chem.* **2006**, *13*, 639−645.
(29) Moro, S.; Bacilieri, M.; Deflorian, F.; Spalluto, G. G protein-coupled receptors as challenging druggable targets: Insights from in silico studies. *New J. Chem.* **2006**, *30*, 301−308.
(30) Moro, S.; Deflorian, F.; Bacilieri, M.; Spalluto, G. Ligand-based homology modeling as attractive tool to inspect GPCR structural plasticity. *Curr. Pharm. Des.* **2006**, *12*, 2175−2185.
(31) Catarzi, D.; Colotta, V.; Varano, F.; Cecchi, L.; Filacchioni, G.; Galli, A.; Costagli, C. Triciclic heteroaromatic systems. Pyrazolo[3,4-*c*]-quinolin-4-ones and pyrazolo[3,4-*c*]quinolin-1,4-diones: Synthesis and benzodiazepine receptor activity. *Arch. Pharm.* (*Weinheim, Ger.*) **1997**, *330*, 383−386.
(32) Casnati, G.; Ricca, A. Synthesis of alkyltryptophans and nor tryptophans. *Gazz. Chim. Ital.* **1963**, *93*, 355−367.
(33) Zhou, Q. Y.; Li, C.; Olah, M. E.; Johnson, R. A.; Stiles, G. L.; Civelli, O. Molecular cloning and characterization of an adenosine receptor: The A_3 adenosine receptor. *Proc. Natl. Acad. Sci. U.S.A.* **1992**, *89*, 7432−7436.
(34) Latini, S.; Pedata, F. Adenosine in the central nervous system: Release mechanisms and extracellular concentrations. *J. Neurochem.* **2001**, *79*, 463−484.
(35) Latini, S.; Bordoni, F.; Corradetti, R.; Pepeu, G.; Pedata, F. Temporal correlation between adenosine outflow and synaptic potential inhibition in rat hippocampal slices during ischemia-like conditions. *Brain Res.* **1998**, *794*, 325−328.
(36) Somjen, G. G. Mechanisms of spreading depression and hypoxic spreading depression-like depolarization. *Physiol. Rev.* **2001**, *81*, 1065−1096.
(37) Martone, M. E.; Hu, B. R.; Ellisman, M. H. Alterations of hippocampal postsynaptic densities following transient ischemia. *Hippocampus* **2000**, *10*, 610−616.
(38) Li, A.-H.; Moro, S.; Melman, N.; Ji, X-d.; Jacobson, K. A. Structure-actvity relationships and molecular modeling of 3,5-diacyl-2,4-dialkylpyridine derivatives as selective A_3 adenosine receptor antagonists. *J. Med. Chem.* **1998**, *41*, 3186−3201.
(39) Kim, Y.-C.; Ji, X.-d.; Jacobson, K. A. Derivatives of the triazolo-quinazoline adenosine antagonist (CGS 15943) are selective for the human A_3 receptor subtype. *J. Med. Chem.* **1996**, *39*, 4142−4148.
(40) Maconi, A.; Pastorin, G.; da Ros, Tatiana, Spalluto, G.; Gao, Z.-G.; Jacobson, K. A.; Baraldi, P. G.; Cacciari, B.; Varani, K.; Moro, S.; Borea, P. A. Synthesis, biological properties, and molecular modeling investigation of the first potent, selective and water-soluble human A_3 adenosine receptor antagonist. *J. Med. Chem.* **2002**, *45*, 3579−3582.
(41) Ji, X. D.; Gallo-Rodrighuez, C.; Jacobson, K. A. A selective agonist affinity label for A_3 adenosine recepotrs. *Biochem. Biophys. Res. Commun.* **1994**, *203*, 570−576.
(42) von Lubitz, D. K. Adenosine and cerebral ischemia: Therapeutic future or death of a brave concept? *Eur. J. Pharmacol.* **1999**, *263*, 59−67.
(43) Novellino, E.; Cosimelli, B.; Ehlardo, M.; Greco, G.; Iadanza, M.; La Vecchia, A.; Rimoli, M. G.; Sala, A.; Da Settimo, A.; Primofiore, G.; Da Settimo, F.; Taliani, S.; La Motta, C.; Klotz, K.-N.; Tuscano, D.; Trincavelli, M. L.; Martini, C. 2-(Benzimidazol-2-yl)quinoxalines: A novel class of selective antagonists at human A(1) and A(3) adenosine receptors designed by 3D database searching. *J. Med. Chem.* **2005**, *48*, 8253−8260.
(44) Colotta, V.; Catarzi, D.; Varano, F.; Melani, F.; Filacchioni, G.; Cecchi, L.; Trincavelli, L.; Martini, C.; Lucacchini, A. Synthesis and A_1 and A_{2A} adenosine binding activity of some pyrano[2,3-*c*]pyrazol-4-ones. *Farmaco* **1998**, *53*, 189−196.
(45) Klotz, K.-N.; Vogt, H.; Tawfik-Schlieper, H. Comparison of A_1 adenosine receptors in brain from different species by radioligand binding and photoaffinity labelling. *Naunyn-Schmiedeberg's Arch Pharmacol.* **1991**, *343*, 196−201.
(46) Mazzoni, M. R.; Buffoni, R. S.; Giusti, L.; Lucacchini, A. Characterization of a low affinity binding site for N6-substituted adenosine derivatives in rat testis membranes. *J. Recept. Sign. Transd. Res.* **1995**, *15*, 905−929.
(47) Ferrarini, P. L.; Mori, C.; Manera, C.; Martinelli, A.; Mori, F.; Saccomanni, G.; Barili, P. L.; Betti, L.; Giannaccini, G.; Trincavelli, L.; Lucacchini, A. *J. Med. Chem.* **2000**, *43*, 2814−2823.
(48) Nordstedt, C.; Fredholm, B. A modification of a Protein-Binding Method for rapid quantification of cAMP in cell-culture supernatants and body fluid. *Anal. Biochem.* **1990**, *189*, 231−234.
(49) Cheng, Y. C.; Prusoff, W. H. Relation between the inhibition constant K_i and the concentration of inhibitor which causes fifty percent inhibition (IC_{50}) of an enzyme reaction. *Biochem. Pharmacol.* **1973**, *22*, 3099−3108.
(50) Pugliese, A. M.; Latini, S.; Corradetti, R.; Pedata, F. Brief, repeated, oxygen−glucose deprivation episodes protect neurotransmission from a longer ischemic episode in the in vitro hippocampus: Role of adenosine receptors. *Br. J. Pharmacol.* **2003**, *140*, 305−314.
(51) Anderson, W. W.; Collingridge, G. L. A data acquisition program for on-line analysis of long-term potentiation and other synaptic events. *J. Neurosci. Methods* **2001**,*108*, 71−83.
(52) Pedata, F.; Latini, S.; Pugliese, A. M.; Pepeu, G. Investigations into the adenosine outflow from hippocampal slices evoked by ischemia-like conditions. *J. Neurochem.* **1993**, *61*, 284−289.
(53) OpenMosix: http://www.openMosix.org (2004).
(54) MOE (The Molecular Operating Environment) Version 2006.08, software available from Chemical Computing Group Inc., 1010 Sherbrooke Street West, Suite 910, Montreal, Canada H3A 2R7. http://www.chemcomp.com.
(55) Stewart, J. J. P. *MOPAC 7*; Fujitsu Ltd., Tokyo, Japan, 1993.

(56) Palczewski, K.; Kumasaka, T.; Hori, T.; Behnke, C. A.; Motoshima, H.; et al. Crystal structure of rhodopsin: A G protein-coupled receptor. *Science* **2000**, *289*, 739−745.
(57) Cornell, W. D. C., P.; Bayly, C. I.; Gould, I. R.; Merz, K. M.; Ferguson, D. M.; Spellmeyer, D. C.; Fox, T.; Caldwell, J. W.; Kollman, P. A. A second generation force field for the simulation of proteins, nucleic acids and organic molecules. *J. Am. Chem. Soc.* **1995**, *117*, 5179−5196.
(58) Levitt, M. Accurate modeling of protein conformation by automatic segment matching. *J. Mol. Biol.* **1992**, *226*, 507−533.
(59) Baxter, C. A.; Murray, C. W.; Clark, D. E.; Westhead, D. R.; Eldridge, M. D. Flexible docking using Tabù search and an empirical estimate of binding affinity. *Proteins: Struct., Funct. Genet.* **1998**, *33*, 367−382.
(60) Halgren, T. Merck Molecular Force Field. I. Basis, form, scope, parameterization, and performance of MMFF94. *J. Comput. Chem.* **1996**, *17*, 490−519.

JM070123V